Peripheral nervous system mediates body-wide stem cell activation for limb regeneration

Duygu Payzin-Dogru[1], Steven J. Blair[1,10], Siddhartha G. Jena[1,10], Sarah E. Wilson[1], Ryan T. Kim[1], Aaron M. Savage[1], Emil Kriukov[2,3], Victor Cat[1], Louis V. Cammarata[4], Vivien Bothe[5], Burcu Erdogan[1], Shifa Hossain[1], Noah Lopez[1], Julia Losner[1], Juan Velazquez Matos[1], Sangwon Min[1], Kelly E. Dooling[1], Adam H. Freedman[6], Bobby Groves[1], Benjamin Tajer[1], Glory Kalu[1], Eric Wynn[1], Alan Y. L. Wong[1], Hani Singer[1], Nadia Fröbisch[5], Petr Baranov[2,3], Jason D. Buenrostro[1,7], Brian J. Haas[7], Isaac M. Chiu[8], Timothy B. Sackton[6], Jessica L. Whited[1,7,9,11*]

[1] Department of Stem Cell and Regenerative Biology, Harvard University, Harvard University, 7 Divinity Ave., Cambridge, MA, USA, 02138
[2] Schepens Eye Research Institute of Massachusetts Eye and Ear, Boston, MA, USA, 02114
[3] Department of Ophthalmology, Harvard Medical School, Boston, MA, USA, 02114
[4] Department of Statistics, Harvard University, Cambridge, MA, USA, 02138
[5] Museum fur Naturkunde Berlin, Berlin, Germany
[6] Informatics Group, Harvard University, 38 Oxford St., Cambridge, MA, USA 02138
[7] The Broad Institute of Harvard and MIT, Cambridge, MA, USA, 02138
[8] Department of Immunology, Blavatnik Institute, Harvard Medical School, Boston, MA, USA, 02115
[9] Harvard Stem Cell Institute, Harvard University, Cambridge, MA, USA, 02138
[10] These authors contributed equally
[11] Lead contact
[*] Correspondence: Jessica L. Whited, jessica_whited@harvard.edu

SUMMARY

Many species throughout the animal kingdom naturally regenerate complex body parts following amputation. Most research in appendage regeneration has focused on identifying mechanisms that influence cell behaviors in the remaining stump tissue immediately adjacent to the injury site. Roles for activation steps that occur outside of the injury site remain largely unexplored, yet they may be critical for the regeneration process and may also shape the evolution of regeneration. Here, we discovered a role for the peripheral nervous system (PNS) in stimulating a body-wide stem cell activation response to amputation that drives limb regeneration. Notably, this systemic response is mediated by innervation at both the injury site and in distant, uninjured tissues, and by several signaling pathways, including adrenergic signaling. This work challenges the predominant conceptual framework considering the injury site alone in the regenerative response and argues instead for brain-body axis in stem cell activation as a priming step upon which molecular cues at the injury site then build tissue.

Keywords: regeneration, systemic responses, peripheral nervous system, adrenaline, mTOR, stem cells, progenitor cells, limb, amputation

INTRODUCTION

Replacing large body parts following severe injury is a long-term goal of regenerative medicine, and one which is likely to stand on first elucidating how other animals execute this enormous task. Regenerative abilities, however, vary dramatically across extant clades. Whether these differences reflect potentially selectable traits in the wild that may be critical for understanding—and potentially provoking—regeneration remains largely undetermined. Salamanders and humans share an evolutionary history as tetrapods (four-limbed vertebrates) and their limbs are anatomically very similar, yet in salamanders they can be spontaneously regenerated throughout life following limb loss in the wild or amputation in the laboratory.[1,2] Recent studies have revealed some clues about the transcriptional regulation accompanying salamander limb regeneration, along with evidence that particular genes and molecules are important to the process.[3-7] However, these studies have thus far not provided critical clues about how organismal-level signaling throughout the body might be integral to regeneration, even though possible systems-level controls in regenerative organisms are beginning to be appreciated[8].

Salamanders, unlike humans and other mammals, grow an essential and outwardly-visible tissue primordium called a "blastema," which contains the progenitor cells required to grow a whole limb. The decision to grow a blastema or not and, potentially, the rate at which the blastema response can be executed is likely to be a critical determinant of whether regeneration happens. Prior studies have shown that invertebrates undergo broad body-wide proliferation before that response becomes restricted to the amputation site, at which point blastema formation becomes apparent.[9-12] Broad activation followed by local blastema formation as a strategy for regeneration could also underlie limb regeneration in vertebrates, but this hypothesis has not yet been tested. If some species do use this strategy to effectively regenerate limbs, the discrete activation and blastema specification steps could be examined in detail in mammals to determine which components might occur despite their overall inability to naturally regenerate limbs. Here, we explored these concepts and defined molecular pathways controlling body-wide activation responses to limb amputation that prime local blastema formation in the super-regenerative axolotl. We find that the peripheral nervous system mediates body-wide stem cell activation in response to amputation and that α-adrenergic signaling is required for systemic activation and priming of cells for limb regeneration, while β-adrenergic signaling promotes localized blastema growth at the injury site.

RESULTS

Amputation primes distant tissues for faster future regeneration

We recently discovered that following axolotl limb amputation, cells located throughout the body, including within contralateral unamputated limbs, proliferate, in a "systemic activation" response.[13] Through amputating limbs and surgically blocking their regeneration, we also showed that systemic activation is an amputation-injury induced response *per se* rather than a consequence of the regeneration process.[13] However, the physiological role of this response in axolotls and/or other salamander species was unknown. Another major outstanding question is what molecular and cellular mechanisms underlie systemic activation in axolotl. Here, we first sought to understand what the consequences of systemic activation are in animals that have recently undergone amputation. We considered whether there could be a need for wild salamanders to sequentially regenerate multiple limbs over a short timeframe. This is conceivable, as limb and tail regeneration following conspecific or predatory bite wounds is frequent in wild salamander populations[14,15] and some salamander species even use a form of tail autotomy[15].

Moreover, fin regeneration is a common feature among lungfish[16], the closest relative of limbed vertebrates. Axolotls (*Ambystoma mexicanum*) are critically endangered in the wild[17] and consequently could not be investigated in a natural setting. We therefore examined tiger salamanders (*Ambystoma tigrinum*), close cousins of axolotls, found in our naturalistic outdoor pond setting, for evidence of simultaneous multiple limb regeneration. We found that, indeed, many larval tiger salamanders had multiple limbs at various states of regeneration in this natural setting (**Figure 1A**; N>6). Being at off-set stages implies that the amputations that produced them occurred sequentially. Indeed, the loss of a first limb might be expected to reduce mobility and perhaps predispose an animal to subsequent predation. This data indicates that in certain settings, limb loss is likely to occur repetitively, and hence to be physiologically relevant for salamanders.

Based on our previous study and this evidence of natural multiple limb regeneration in salamanders, we hypothesized that following a first amputation, distant tissues harboring systemically-activated cells might exhibit accelerated local regeneration kinetics. We therefore challenged axolotl limbs in a systemically-active state to a local amputation 7 days after contralateral amputation (**Figure 1B**). We found that limbs engaged in systemic activation regenerate faster than those limbs on naïve animals that had never undergone amputation (**Figure 1C-D**). We observed this effect to be significant at the early initiation stages of regeneration (**Figure 1D**) when the blastema is being built. The effect continued through later stages of regeneration, when the blastema commences differentiation (**Figure 1E**), and digits become discernable (**Figure 1F**). We also tested whether molecular markers of blastema formation are accelerated following amputation of primed limbs versus naïve limbs. We performed HCR-FISH to detect *Prrx1* mRNA expression[18] at 5 days post-amputation (dpa) (**Figure 1G**), and we observed a significant increase in the signal intensity of this blastema-cell marker in the primed limbs versus naïve limbs (**Figure 1G-H**). This data supports the conclusion that amputation-induced systemic activation leads to priming of distant tissues for faster regeneration when subjected to future local injury. A faster recovery of digits, for example, may be critical for survival in the wild.

We also investigated how many divisions cells undergo following their systemic activation and how long the priming effect lasts. Using a short-pulse (EdU) and long-chase strategy, we found most labeled clones in limbs to be composed of 2-8 cells (**Figure 1I**), indicating amputation-induced proliferation may last only a few cell cycles. Concordantly, we found there to be no difference in the fraction of EdU+ cells by 6 weeks post-amputation (**Figure 1J**). We also found that systemically-activated limbs challenged with local amputation 4 weeks after initial activation regenerated at the same rate as naïve limbs, indicating the effect is relatively short-lived (**Figure 1K-M**).

The peripheral nervous system is a conduit for systemic proliferative response to amputation

Determining how amputation-induced signals spread throughout the body is important for unraveling the molecular and cellular mechanisms of the systemic activation response. We hypothesized that the peripheral nervous system (PNS) might be a conduit for this type of information, as it rapidly transduces sensory afferent information to the spinal cord and brain, as well as sends motor and autonomic efferent signals from the brain to the body, thereby facilitating communication between distant anatomical locations. We tested whether systemic activation requires peripheral innervation at either the responding site (**Figure 2A-E**) and/or the amputation site (**Figure 2F-G**) using surgical denervation (via brachial plexus nerve transection or sciatic nerve transection) and sham operation controls (**Figure S1A**). We found that systemic activation did not occur when these distant sites contralateral to amputation were denervated at the time of the amputation injury (**Figure 2A-B**). As a control, we found that systemic activation still occurred following amputation when these distant sites (contralateral limbs) underwent sham operations. We parsed the contralateral tissues into three broad tissue categories—epidermis,

skeletal elements, and internal (non-skeletal, soft) tissues—and quantified the extent of systemic activation within each (**Figure 2C-E**). This analysis revealed that each of these three categories of tissue types requires an intact nervous system for cellular activation. We also found that when limbs were denervated and then immediately amputated, the amputation no longer provoked systemic activation in distant sites (contralateral limbs) (**Figure 2F-G**). Sham surgeries in which limbs were not denervated prior to their amputation still provoked the systemic activation response. These results demonstrate that peripheral innervation of both the amputated limb and the distantly-responding limb are required for systemic activation of progenitor cells. Therefore, both neuronal input that senses injury and neuronal output that mediates efferent signaling to tissues could regulate systemic activation.

To explore molecular pathways that may underlie PNS dependence in responding tissues, we performed two types of bulk RNA-seq transcriptional analyses. We compared gene expression in limb nerve bundles from animals actively engaged in systemic activation to those who failed to systemically activate due to denervation (**Figure 2H**). We identified 273 genes showing significant differential expression between these two conditions (**Figure 2H**, **Table S1**). We also performed differential gene expression analysis between samples derived from the soft tissue of systemically-activated limbs and the soft tissue of limbs that were denervated and, therefore, not activated (**Figure 2K**). This analysis identified 82 differentially-expressed genes (**Figure 2I**, **Table S1**). We then used the candidate genes revealed by the RNA-seq of nerve and surrounding tissue to functionally test pathways to determine if they are required for systemic activation. We prioritized well-studied pathways with robust pharmacological inhibitors.

α-Adrenergic signaling drives systemic activation and priming

Adra2a, which encodes α-2A adrenergic receptor, was 7.4-fold upregulated in transected nerve samples, which are deficient in stimulating systemic activation, when compared to intact nerves (**Figure 2J**, **Table S1**), implicating a possible role for adrenergic signaling in the systemic activation response to amputation. Dorsal root ganglia (DRG) harbor the cell bodies of peripheral sensory neurons that innervate peripheral tissues including limbs. We mined an existing axolotl DRG scRNA-seq dataset that we previously collected[19] and found that several types of peripheral sensory neurons express adrenergic receptors in homeostasis (**Figure S1B**). The primary neurotransmitters that drive adrenergic signaling are the catecholamines adrenaline and noradrenaline, which are elevated during stress response.[20] We, therefore, quantified levels of these molecules in axolotl plasma using ELISA. We found that while circulating plasma levels of noradrenaline are similar between unamputated axolotls and axolotls at four hours post-amputation (**Figure 3A**), the amputated animals exhibited approximately 2-fold more adrenaline in plasma compared to unamputated controls (**Figure 3B**). Enzymes in the adrenaline biosynthesis pathway are also expressed by some axolotl DRG neurons, (**Figure S1C**) also mined from our work.[19] To address function, we treated axolotls with yohimbine, a well-studied ADRA2A antagonist,[21,22] to test for an adrenergic signaling requirement in both the regenerating limb and in systemic activation. We found that in animals treated with yohimbine, amputated limbs had lower numbers of proliferating cells (**Figure 3C-D**), and limbs contralateral to amputation did not undergo systemic activation (**Figure 3E-F**), demonstrating that adrenergic signaling is required for robust cell proliferation at the injury site and for systemic stem cell activation in response to amputation. We then asked whether adrenergic signaling is also required for priming distant tissues for future regeneration (**Figure 3G**). We found that when axolotls were treated with yohimbine from 2 days before to 7 days after amputation, priming was diminished (**Figure 3H**), with both initial blastema growth (**Figure 3I**) and limb differentiation (**Figure 3J**) occurring more slowly. We tested whether stimulating adrenergic signaling via

the alpha-2a adrenergic agonist clonidine might enhance priming, and we found evidence that this pathway can indeed be stimulated to accelerate the regeneration of distant tissues that have been systemically activated (**Figure 3K-M**). Our finding that α2-adrenergic-receptor signaling mediates systemic activation prompted us to ask whether β-adrenergic-receptor signaling also contributes to systemic activation. We, therefore, used an identical treatment regimen to administer the non-selective β-adrenergic receptor antagonist propranolol[23] to axolotls (**Figure 3N-P**). We found that while propranolol treatment led to a significantly decreased fraction of cells actively in S-phase within blastemas of regenerating limbs (**Figure 3N-O**), it had no effect on systemic activation (**Figure 3N, 3P**). These results indicate that α-adrenergic signaling is required for the systemic activation response to amputation in axolotls, whereas β-adrenergic signaling is only required for the localized cellular proliferation response at the amputation site. We next asked whether stimulating α-adrenergic signaling in the context of a single limb amputation alone is sufficient to promote faster blastema formation, and, using clonidine treatment, we found that this was the case (**Figure 3Q-R**). This enhanced regeneration response is accompanied by an increased fraction of proliferating cells in the amputated limbs (**Figure 3S-T**). We also tested whether clonidine administration is sufficient to promote systemic activation in the absence of amputation injury. We found that clonidine treatment alone was insufficient (**Figure S1D-E**). Clonidine treatment also could not rescue systemic activation if either amputated limbs (**Figure S1F-G**) or responding limbs (**Figure S1H-I**) were denervated. Together, these results argue that systemic activation and priming require α-adrenergic signaling, and that stimulating this pathway is sufficient to promote limb regeneration, but it likely acts in concert with other pathways downstream of nerves. They also argue that β-adrenergic signaling is likely required specifically at the injury site to promote limb regeneration.

Systemically-activated cell types are shared with proliferating cell types in homeostasis

Defining which cells are activated is key to developing hypotheses about how systemic activation relates to regeneration and function. It is possible that systemic activation may accelerate the regeneration of specific cell types more effectively, or it may be unbiased in its effects. We therefore asked which types of cells become systemically activated in response to amputation. To account for the full repertoire of activated cells that we observed, we turned to an agnostic method of addressing this question. We used FACS and the nuclear stain Hoechst to sort cells with 4C nuclear content from systemically-activated limbs and from homeostatic limbs (**Figure 4A-B**). The fraction of 4C versus 2C cells was considerably higher in activated samples (14.53%) versus homeostatic samples (5.84%) (**Figure 4B**). We identified cell types in both samples via single-cell RNAseq and downstream clustering analyses (**Figure 4C**, **Table S2**). The distribution of marker gene expression across clusters is shown in **Figure S2A**. In the systemically-activated samples, we found multiple blood cell types, including myeloid progenitors, T cells, two clusters of hematopoietic progenitors, and two clusters of red blood cells (**Figure 4C**). We also identified skeletal muscle progenitors, two types of endothelial cells, basal epidermal cells, and four other types of epidermal cells (**Figure 4C**). We parsed eight subtypes of activated fibroblasts (**Figure 4C**). Intriguingly, the same clustering algorithm applied to the 4C cells purified from homeostatic animals produced the same number and repertoire of cell clusters (**Figure 4D**). One notable difference was the fibroblast VII population, which appeared in both conditions but in slightly different locations on the UMAP. This result indicates that axolotls systemically activate the same cell types that cycle during homeostasis, boosting the number of these cells actively in S-phase after amputation.

We performed differential gene expression analysis between the two conditions for each cell cluster (**Figure 4E, Table S3**). Cell types for which we uncovered any number of significant differential gene expression included two fibroblast cell types, two types of epidermal cells, basal keratinocytes, two

types of endothelial cells, red blood cells, erythrocyte progenitors, two types of immune cells, myeloid progenitor cells, and hematopoietic progenitor cells (**Figure 4E**). We focused on fibroblasts because they are known to play a central role in contributing to blastema formation during limb regeneration,[24,25] and connective tissues have been shown to exhibit more plasticity across the limb regeneration process than other tissues.[26,27] We identified 19 genes to be significantly ($p<0.05$) different in expression between systemically-activated type IV fibroblasts versus 4C type IV fibroblasts from homeostatic animals (**Figure 4F**), while an additional 44 genes were differentially expressed with $0.05<p<0.1$. We detected no significant differences in gene expression in other fibroblast cell types between systemically-activated and correlating 4C cells from homeostatic animals (other than a single unannotated gene whose expression differs among the two conditions in fibroblast II). For the type IV fibroblasts, 8/19 genes with $p<0.05$ and 20/44 genes with $0.05<p<0.1$ are predicted to encode ribosomal subunits (**Figure 4F**, **Table S3**). 27/28 of these ribosomal subunits were more highly expressed in systemically-activated fibroblast IV cells than their 4C homeostatic counterparts. The most significant differentially expressed gene ($p<0.0059$) to display this relationship is predicted to encode Snail (SNAI1) (**Figure 4F**), a factor most known for its promotion of epithelial-to-mesenchymal transition (EMT) in a variety of contexts,[28-30] which was expressed 1.6-fold higher in systemically-activated fibroblast IV cells. We also found the p53 inhibitor Sestrin 1[31] (SESN1), which regulates mTORC1 and mTORC2 in other species by acting as a nutrient sensor,[32] to be significantly upregulated ($p<0.0059$), with a 2-fold enrichment in the systemically-activated fibroblast IV cells compared to their 4C homeostatic counterparts (**Figure 4F**).

We further characterized our 4C fibroblast populations using an existing dataset that compared fibroblast populations in the regenerative reindeer antler (velvet) skin and the non-regenerative reindeer back skin (**Figure 4G**).[33] As expected, axolotl fibroblasts most closely resemble reindeer fibroblasts (Wilcoxon rank sum test with continuity correction, $W = 784$, p-value $< 2.2e-16$) (**Figure S2B**). In homeostasis, several proliferating axolotl limb fibroblast populations, such as fibroblast II, III, IV and VI, have a “fibrotic” gene signature, based on their similarity to reindeer back skin, whereas axolotl fibroblast V, VI, and VII have a “regenerative” gene signature, based on their similarity to reindeer antler skin. Upon amputation, we found that regardless of their initial status, almost all 4C fibroblast populations shifted to a more regenerative gene signature; though they are distant from the amputation site, these axolotl cells more closely resemble the regenerative profile underlying reindeer antler fibroblasts post-injury (**Figure 4G**). We performed a similar analysis for the 4C epidermal cell populations and found that proliferating epidermal cells in both the homeostatic and systemically-activated axolotl limb most closely resemble regenerative reindeer antler basal keratinocytes at post-injury time points (**Figure 4F**).

To gain insights into possible cell state trajectories, we used the 4C scRNA-seq dataset and RNA Velocity to predict putative cell fate trajectories (**Figure S2C**).[34] In both homeostatic and systemically-activated conditions, we found evidence for fibroblast II and IV populations potentially transitioning to fibroblast I cell state, which might be enhanced in the systemically-activated samples (**Figure S2C-D**). Genes that are most likely driving these changes are highlighted in **Figure S2E**; notably, nearly all of these genes remain unannotated in the axolotl genome, with no known high-confidence orthologs. Similarly, applying gene dynamics analysis to the 4C cells dataset identified a handful of transcripts with unique regulation in the kinetics of RNA transcription and splicing (**Figure S2E**), although we again found almost all of these genes to be unannotated.

We additionally analyzed the single cells not undergoing systemic activation, those with 2C nuclear content (**Figure 4I**). We did not find any difference in the repertoire of cell types from these two conditions, 2C cells from homeostatic versus 2C cells from activated limb samples (**Figure 4J, Figure S2D**). Major transcriptional differences were observed mainly within the epidermal cell populations and small secretory cell populations (which reside in skin), indicating that a global transcriptional reprogramming of skin may occur downstream of amputation (**Figure 4K, Table S5**). We further

performed cross-species analysis with the reindeer datasets and found that axolotl 2C fibroblasts have more similarity to reindeer fibroblasts during homeostasis (**Figure 4G**) than to reindeer fibroblasts post-injury. Additionally, axolotl 2C epidermal cells harvested from the homeostatic and activated limb more closely map to post-injury reindeer basal keratinocytes in the antler rather than those in the back (**Figure 4H**).

We further mined the expression of transcripts encoding adrenergic receptors in our single-cell RNA sequencing datasets, and we found evidence they are expressed in many types of 4C cells in our dataset (**Figure S3**). Collectively, the data indicate that amputation induces a subset of cell types throughout the body that ordinarily can proliferate during homeostasis to become hyper-proliferative, thus becoming systemically activated.

Chromatin accessibility changes associated with systemic activation

We hypothesized that cells might be altering their chromatin accessibility in response to amputation as a means to shift into an activated state primed for regeneration. For example, a recent study uncovered activation of a gene-specific enhancer in the brains of zebrafish following cardiac damage and implicated this region in cardiac response[35]. To address this possibility, we used our FACS strategy to isolate 4C cells from the homeostatic, systemically-activated, and regenerating limb samples, including blastema and wound epidermis. We pooled cells from each of these three conditions and performed ATAC-seq. We performed a global analysis to identify transcription factor binding sites within regions of open chromatin across all three populations (**Table S6**). In comparing these data across the three populations, we identified enriched motifs that are shared among two conditions and motifs shared between all three conditions (**Figure 5A**). Notably, 95 motifs were exclusively shared between activated and blastema 4C populations. These motifs represent potential transcription-factor binding sites common to cells that proliferate in response to amputation regardless of their vicinity to the injury site (**Figure 5A**, **Table S6**). Among these motifs shared between 4C systemically-activated and 4C blastema cells are putative binding sites for the canonical tumor suppressor proteins p53 and WT1. Strikingly, no motifs were exclusive to the intact sample (**Figure 5A**, **Table S6**), while 229 motifs are shared across all three samples. These 229 motifs may represent binding sites for transcription factors associated with generalized cellular proliferation in 4C cells in the axolotl. We found that 97 motifs are exclusively enriched in the open conformation in the blastema samples. These loci may, therefore, be of interest as the presumably “blastema-unique” regions of chromatin accessibility that potentially distinguish cells that proliferate in response to injury from those that proliferate and also undergo blastema cell state specification. However, with these data alone, distinguishing this scenario from instances in which a cell may have transitioned to a blastema state and then later initiated or continued proliferation is not possible. Our analysis also identified 40 motifs that are unique to systemically-activated cells and not shared with 4C cells from homeostatic or blastema samples. These sites may be of special interest in understanding how cells at distant sites to a lost limb are restrained from becoming blastema cells, and/or how they might otherwise influence local tissue dynamics to prevent ectopic blastema formation. Among these sites, we identified several putative binding sites for transcriptional activators and repressors with well-established roles in patterning vertebrate limbs, such as the homeodomain-containing proteins En1, Lhx9, and Pitx1[36-41].

We initially examined common transcription factor binding sites between regenerating and systemically-activated limbs as they might share features. Specifically, we explored the enrichment in open chromatin observed for putative p53 binding sites common to the systemically-activated and blastema samples. We intersected the predicted p53 binding sites in the axolotl genome with our ATAC-

seq data, and we identified 102 genes with transcriptional start sites within 3kb of these motifs within open chromatin. We further intersected these data with our 4C single-cell RNAseq data, and we identified 72 of these 102 genes to be expressed in our 4C samples, 58 of which are more highly expressed in systemically-activated fibroblast populations versus homeostatic 4C fibroblast populations (**Figure 5B**). Among these 58 genes is ADRA2A (**Figure 5B**), indicating ADRA2A may be a transcriptional target of p53 in the process of systemic activation and priming for limb regeneration. We considered whether p53 might be transcriptionally upregulated systemically following amputation; however, we did not find this to be the case (**Figure S4**). However, p53 activity is known to be post-transcriptionally regulated in a variety of contexts[42]. Given these data, we tested whether global levels of p53 activity might be higher in systemically-activated axolotls compared to homeostatic controls. We introduced an established p53 activity reporter[43,44] into axolotl limbs and tested whether signal is higher in the systemically-activated state (**Figure 5C**). We found that p53 activity is significantly higher in systemically-activated axolotls compared to naïve, homeostatic animals (**Figure 5C**), indicating it is possible axolotls globally upregulate tumor suppressors in response to limb amputation.

Next, we focused on factors that are enriched in the systemically-activated but not homeostatic and regenerating limbs. A previous study investigated TGF-β signaling and its SMAD effectors at the local injury site during axolotl limb regeneration[45], but the potential roles of these factors in global activation were not investigated. We therefore performed the same analyses on SMAD3, as we observed this transcription factor's binding sites to be enriched in open chromatin specifically in the systemically activated cells, but not in the 4C homeostatic nor blastema samples. We found evidence that the repertoire of SMAD3 transcriptional targets may be vast within systemically-activated cells, with 4841 genes as putative targets. Given this large number of potential target genes, we performed GO analysis to identify biological pathways that may be regulated by SMAD3 in systemically-activated fibroblasts (**Figure S5A**). Among the significant GO terms associated with genes expressed in 4C fibroblasts with putative SMAD3 binding sites, we identified "regeneration," "G protein-coupled receptor signaling pathway," "DNA damage response" as well as two GO terms associated with p53 activity, and several GO terms associated with and insulin-like growth factor signaling (**Figure S5A**).

Insulin/IGF signaling is also required for systemic activation and limb regeneration

We further explored specific genes in the insulin/IGF signaling pathways that may act downstream of SMAD3 in systemically-activated cells. We found a putative SMAD3-binding site immediately upstream of the *Foxo1* transcriptional start site. FOXO1 is a transcription factor that acts downstream of insulin and IGF signaling in a variety of other contexts[46-48]. We found minimal differences in active transcript expression between homeostatic and activated 4C cells with respect to *Foxo* genes (**Figure S5B**), suggesting that while they may be poised for expression, they may not yet be transcriptionally upregulated. We therefore hypothesized that *Foxo1* expression may be queued in a later step in regeneration, after cells have been systemically activated, and that its function may be required for blastema formation and limb regeneration. We pharmacologically inhibited FOXO1 to test this possibility using the well-characterized drug AS1842856,[49,50] and we found that axolotls treated with this drug exhibit dramatic inhibition of limb regeneration (**Figure S5C-D**).

The insulin/IGF pathway hits from ATAC-seq analyses also provided a connection to some of our bulk nerve RNA-seq and scRNA-seq findings. *Igfr1* was differentially regulated in surrounding tissues of denervated limbs versus sham-operated limbs following amputation (**Table S1**). We applied CellChat to the 4C fibroblast populations in our single-cell dataset to better understand what pathways they may use to signal one another. CellChat predicted a likely role for insulin/IGF signaling in regulating cell-cell communication in 4C fibroblasts in systemic activation (**Figure S5E-F**). Inhibition of IGF1R by NVP-

ADW742,[51] an ATP-competitive inhibitor, blocked systemic activation in limbs contralateral to amputation, indicating IGF-1 signaling is necessary for this process (**Figure S5G-H**).

Not all pathways exhibiting changes at the transcriptional levels in our analyses are required for systemic activation. For example, we tested WNT signaling as *Lef1* was differentially regulated in nerves following denervation and contralateral amputation (**Table S1**). Although WNT signaling has been implicated in a variety of regenerative events across many species,[52-56] we found the canonical pathway to be dispensable for systemic activation in axolotl as the WNT inhibitor IWR-1[57] did not alter the number of cells that become systemically activated in response to amputation (**Figure S5G-H**).

These experiments underscore that multiple pathways act in concert to systemically activate cells. However, there is specificity to this system as some prominent developmental signaling pathways, such as WNTs, are dispensable for systemic activation and therefore likely contribute toward other aspects of limb regeneration.

An evolutionarily conserved role for mTOR and related signaling pathways in axolotl systemic injury responses?

Our data thus far supports a critical role for the PNS and adrenergic signaling in the systemic proliferative responses to amputation injury in axolotl. As mice have been shown to engage in a similar response following more limited local injuries,[58] the possibility that the first step of limb regeneration—in which cycling progenitor cells shift from a homeostatic function to a regenerative function—is operational in mammals exists. This activation in mice has been attributed to circulating Hepatocyte growth factor activator (HGFA) that activates HGF in distant tissue stem cell niches, which in turn bind the cMET receptor, activating downstream mTOR signaling.[58,59] Any role for PNS in controlling this pathway in mice has not been reported, but examining mTOR signaling in axolotl, potentially separable from the PNS, would be important from a comparative standpoint. mTOR signaling and insulin signaling are also intimately coupled in many biological settings, for example, mTORC1 is activated downstream of insulin signaling[60-62]. We showed insulin/IGF signaling is required for systemic activation, providing more support for exploring mTOR in axolotl systemic activation. Additionally, a recent study of the amputation site identified a key role for mTOR in translational regulation of the wound-healing stage of axolotl limb regeneration[63].

Given these considerations, and since we had previously shown that mTOR signaling is upregulated in distant tissues, such as contralateral limbs, during systemic activation in the axolotl,[13] we investigated the possibility that mTOR might also be functionally important for systemic activation in axolotl. Using CellChat, we found substantial differences in HGF signaling in 4C cells engaged in systemic activation versus 4C homeostatic cells (**Figure S6A**).[58,59,64] Of note, we also uncovered relationships between other cell types, such as hematopoietic progenitors and skeletal muscle cells. This finding may reflect a parallel mechanism in axolotl to what was previously described in published work in the mouse whereby activation responses can be mediated by the bloodstream[59,65]. Additional possible signaling relationships we have uncovered between cell types include epidermal cell to blood cells, and epidermal cell to fibroblasts (**Figure S6A**). These putative relationships will require future experimental investigation; however, since HSCs may be molecularly communicating with skeletal muscle progenitor cells, determining if this relationship is conserved with the one reported in mice[59] will be important. We found axolotls treated with the mTOR inhibitor rapamycin[66] regenerate limbs more slowly (**Figure S6B-D**), with lower numbers of proliferating cells in the blastema (**Figure S6E-F**), and that both systemic activation and priming are inhibited by rapamycin treatment (**Figure S6G-L)**. Considering the role of mTOR in nutrient sensation, cell growth, and proliferation,[67] we tested whether fasted axolotls exhibit altered levels of systemic activation and whether cell proliferation in this context might additionally be regulated by

mTOR signaling, adrenergic signaling, or both. We found that global cell proliferation rates in fasted axolotls with amputation were dramatically lower than typically observed in well-fed axolotls (**Figure S6M-N**). Yet, we found that in the context of an amputation, the number of these proliferating cells at distant sites was still sensitive to mTOR signaling, but they may not be influenced by adrenergic signaling (**Figure S6O-P**). We also examined mTOR activation in dorsal root ganglia (DRG), which include somatosensory neurons that innervate and receive sensory input from the limbs (**Figure S6Q**).[68] While there was no significant difference in the proliferation of cells in the DRGs following amputation (**Figure S6R**), we found that neurons in DRGs from both amputated limbs and contralateral limbs showed higher levels of mTOR activation than those from homeostatic limbs (**Figure S6S**). These results demonstrate that mTOR signaling is important for systemic activation responses to limb amputation in axolotl, although this dependency may represent evolutionary conservation or convergent evolution when considering a similar—but not identical—phenomenon in mice (discussed below).

DISCUSSION

Our results highlight a previously-unappreciated role for body-wide activation of cell types that cycle during organismal homeostasis and their repurposing for pro-regenerative responses during vertebrate limb regeneration. These findings have important implications for regenerative biology from several perspectives.

Our work implores a re-evaluation of the initiation phase of limb regeneration, demonstrating important steps that are separable in both time and space. Nearly all previous work investigating regeneration initiation has focused exclusively on effects at the local injury site. We had previously demonstrated that axolotls respond to amputation by systemically activating a subset of cells to re-enter the cell cycle, but that work did not address the mechanisms of this response or, importantly, the implications of it for limb regeneration. This study demonstrates that systemic activation is a priming step in the regenerative process, on which subsequent cell behaviors necessary for blastema creation and, ultimately, regeneration are built. Our work highlights that connecting global events to local signaling and cell behaviors is crucial to understanding the regeneration process and how it may have been shaped over evolutionary time.

We have here established that systemic stem cell activation is a key feature of the early regenerative response, thus highlighting the importance of understanding how this process is stimulated by amputation. Our data support a model in which the mechanism of systemic activation requires peripheral innervation at both the injury and distant responding sites (**Figure 6A**). Our work identifies a more primary role for peripheral innervation in the initial stimulation of progenitor cells to re-enter the cell cycle. This role for the PNS is complementary to the previously-appreciated roles for the PNS as a source of mitogens in growing nascent blastemas larger[69-73] and as a positive regulator of limb size during regeneration.[74] We investigated the mechanisms whereby systemic activation occurs, and we discovered adrenergic signaling as a critical mediator of both systemic activation and priming for future regeneration.

Additionally, our findings may provide potential insights into the evolution of regeneration by illustrating the possible advantage of systemic activation being a primary response to amputation. While this initial global activation event poises cells at the injury site toward a regenerative response, it simultaneously poises other tissues in the body toward accelerated regeneration should it become necessary. This global priming could have direct relevance in the wild for animals faced with intense predation—either from heterospecific or conspecific predation. Indeed, this might already have been of relevance in the stem lineage of modern amphibians some 290 Ma ago, as fossil evidence not only suggests that these ancient amphibians were capable of regeneration, but also that regeneration had occurred in more than one limb in single specimens[14].

Axolotls are neotenic, and, in the wild, they live their entire lives in the water; however, this neotenic life cycle is a derived trait.[75] For most species of salamanders, eggs are laid at very high density in a short time frame (for example, in vernal pools in the spring), resulting in high densities of larval salamanders and cannibalism.[76] Because of these circumstances, and in conjunction with our direct evidence, salamanders may need to regenerate multiple limbs in a short time frame, especially if these limbs are necessary for more mature salamanders to leave the water for their terrestrial habitats. Thus, though outside the scope of this study, evaluating the potential adaptive value of systemic activation to salamanders in a natural setting, while a tantalizing possibility, will require controlled experimentation, including fieldwork. The possibility that systemic activation initiates limb regeneration in wild salamanders while also preparing other appendages for future regeneration is salient.

Several other outstanding questions remain for understanding the implications of our findings. We postulate that while the initial proliferative response to amputation is global in axolotls, the sustained proliferation of activated cells and their migration out of tissue niches will be driven by local cues, potentially wound-epidermis factors (**Figure 6B**). Understanding how wound epidermis-derived cues influence the biology of systemically-activated cells will be important. Additional experimentation will also be required to address the relative contributions of sympathetic neurons locally versus the hypothalamic-pituitary-adrenal (HPA) axis as the source of the catecholamines important for regeneration. While we showed that the systemic activation and priming effects are transient and disappear within several weeks, the mechanism whereby they are extinguished remains to be determined, and defining the precise roles of epigenetics in this process requires more experimentation.

Our findings suggest body-wide regulation of p53 activity may be involved in systemically activating fibroblasts, and/or in controlling their behaviors post-activation, perhaps via regulation of adrenergic signaling. However, additional experiments are required to fully elucidate these connections. Previous studies have found p53 mRNA transcripts and activity to be downregulated at the amputation site in the early phases of axolotl limb regeneration[43,77], but the possible regulation of p53 body-wide in response to amputation had not been investigated. We found that axolotls in a systemically-active state have enhanced p53 activity at sites in the body distant from the amputated limb; this effect may be widespread, potentially global. This finding is particularly intriguing since salamanders are often described as cancer-resistant.[78-83] Newts have been reported to recover from experimentally-induced, multi-site, body-wide metastatic skin cancer by differentiating tumors into normal tissue.[84] This observation aligns with Waddington's "Cancer and the Theory of Organizers" hypothesis describing "individuation fields" which, in highly-regenerative animals, might act to reduce cancer susceptibility by directing cells toward differentiation.[84,85] Future work may uncover a connection between systemic activation and tumor formation, considering several of the transcription factors whose binding sites we identified as enriched in both blastema and systemically-activated cells are known to be tumor suppressors in other biological contexts[86,87]. In some contexts, regulation of these tumor suppressors has been observed in signaling pathways we show are crucial for systemic activation[88,89].

While systemic activation may have short-term benefits to the organism by acting to prime other tissues for regeneration, and possibly by modulating global tumor suppressor activity, the consequences of this system over an individual lifespan need to be evaluated. Repeated injury and chronic stimulation of this system may come at a cost. We previously demonstrated that even the axolotl's limb regenerative abilities can be compromised by repeated amputation-regeneration cycles,[90] as is also the case in at least one species of newt;[91] hence, investigating how regenerative decline provoked by repeated injury interfaces with systemic activation will be interesting. While we speculate here that an EMT-like process might be primed in systemically-activated cells and employed by them to construct a blastema should a local injury arise in the future. However, EMT-like gene regulatory networks can also contribute to fibrosis and scarring[92]. Therefore, an alternative hypothesis, that upregulation of genes tied to EMT could be a

means for the organism to counteract distant cell activation and thereby prevent ectopic blastema formation, should also be considered.

Our work will likely have important implications for defining where, in the process of limb regeneration, mammals have evolved and/or retained additional molecular controls that restrict natural regenerative ability. While we found mTOR signaling is also required for the systemic activation response we have studied in axolotl, the process is clearly different from in mouse, and these differences are likely critical. These results highlight the need to understand how mTOR signaling in sensory neurons might influence systemic activation and priming, and they support future exploration of how the PNS could interface with circulation in controlling body-wide stem cell responses to amputation. Together, this work and our previous study[13] both show that while mTOR is upregulated in axolotls during systemic activation, the cells that activate mTOR in distant locations are not the same cells re-entering the cell cycle—only in the blastema itself does mTOR activation and cell-cycle re-entry seem to overlap. This suggests non-cell-autonomous roles for mTOR in systemic activation in axolotl likely underlie the dependency on mTOR for this process. In contrast, in the similar phenomenon reported in mice, cells that upregulate mTOR at distant locations are the same cells entering the "G-alert"/activated state[58,59]. One exciting interpretation of our starvation/mTOR data is that limb regeneration occurs at the expense of growing the body larger or replenishing cells elsewhere in the body lost to normal wear-and-tear. Evaluating this possibility requires future experimentation, but doing so promises to shed light on the "trade-offs" that may be associated with regeneration.

Overall, our work demonstrates that investigating the biology of systemic activation can be an effective means to unravel the key pathways used to prime cells for limb regeneration. Our work predicts that activating the relevant cell types and directing them toward a regenerative response could be stimulated by harnessing adrenergic, insulin, and mTOR signaling in a mammalian setting, providing a major advancement toward the goal of therapeutic limb regeneration in the future. Our findings may also provide important reference points for medical applications outside of the amputee population, for example, in the context of "polytrauma," in which a patient suffers severe wounds in several different body parts.[93]

Limitations of the study

While we find the body-wide proliferative response to reset to homeostasis at 6 weeks post-amputation, it remains to be determined whether epigenetic changes we observed may persist beyond this period or, perhaps, permanently. The relative contributions of circulating epinephrine (as a function of the hypothalamus-pituitary-adrenal axis) versus localized epinephrine signaling (from sympathetic neurons or, potentially, from sensory neurons) to systemic activation and priming remains to be determined. Whether an important role for the PNS in orchestrating the body-wide activation response in mammals also exists, perhaps intertwined with the circulation, remains to be determined. Additional studies will also be required to reveal if either (or both) axolotls and mice reserve some subset of these homeostatic progenitor cell types exclusively or preferentially for regeneration. The mechanistic and evolutionary relationships between the phenomena we describe here and those that operate post-amputation in mammals must also be evaluated.

ACKNOWLEDGMENTS

This work was supported by The Richard and Susan Smith Family Odyssey Award (J.L.W.), the NIH New Innovator Award DP2HD087953 (J.L.W.), NICHD R01HD095494 (J.L.W.), NICHD R01HD115272 (J.L.W.), NSF-CAREER IOS-2145925 (J.L.W.), Harvard University Faculty of Arts and Sciences (J.L.W.),

Harvard/MIT Joint Basic Program in Neuroscience (J.L.W. and I.M.C.), the Human Frontiers Science Program Long-term Postdoctoral Fellowship (A.M.S.), the Harvard Program for Research in Science and Engineering (S.H. and J.L.), the Harvard College Research Program (S.H. and A.Y.L.W.), and the Harvard Stem Cell Institute (A.Y.L.W.). We thank Dr. Elaine Fuchs' lab for sharing reagents. We thank Samantha Payne, Solsa Cariba, Sydney Chambule, Fabiana Duarte, Juliana Babu, Jeramiah Smith, Nataliya Timoshevskaya, Tomás Gomes, and Adnan Abouelela for technical assistance. We thank Brianna Blackmore, Kara Thornton, Lauryn Wilson, Hayden Graham, Damian Bernard, Nicholas Cardelia, Erin Anderson, Vicky Yan, Omenma Abengowe, Rui Qun Miao, Mak Famulari, Nicole Mejia, Madison Hurley, Gregory Gundberg, William Ye, Tyler Mourey for animal care. We thank Ya-Chieh Hsu, Mansi Srivastava, Matthew Warman, Marc Kirschner, Davie Van Vactor, Paola Arlotta, Rich Lee, Paul Garrity, Cliff Tabin, and members of the Whited, Chiu, Greer and Lehoczky labs for discussions and comments on the manuscript. We thank Yulia Swartz for sharing reagents and assisting in data interpretation, and the Bauer Core Facility at Harvard University for cell sorting and sequencing.

AUTHOR CONTRIBUTIONS

D.P.-D, S.E.W., B.E., R.K., S.H., J.L., J.V.M, I.M.C., and J.L.W. designed the experiments; V.B. and N.F contributed tiger salamander data; D.P.-D. S.G.J., S.J.B., S.E.W., E.K., L.C., and J.L.W. wrote the paper; S.G.J., S.J.B., E.K., A.H.F., P.B., B.J.H, and T.B.S. designed and performed computational analyses; L.C. performed statistical analyses; D. P.-D., S.E.W., A.M.S., R.K., B.E., N.L., S.M., B.G., K.D., S.H., J.V.M., A.W., J.L., and H.S. performed sample preparation, experiments, and experimental data analyses. All authors contributed to manuscript editing.

DECLARATION OF INTERESTS

JLW is a co-founder of Matice Biosciences. Other authors declare no competing interests.

MAIN FIGURE TITLES AND LEGENDS

Figure 1. Systemically-activated cells are primed for future regeneration events. (A) Tiger salamander housed in a near-naturalistic pond simultaneously regenerating three limbs (arrowheads). **(B)** Experimental design. We compared regeneration rates of systemically-activated and naïve, control limbs. Green dots, activated, EdU positive nuclei. **(C)** Representative images of regenerating systemically-activated or control limbs (ventral view). **(D-F)** Quantification of blastema area at 14 dpa **(D)**, number of differentiating limbs **(E),** and number of digit outlines **(F)** at 25 dpa (n=15 animals for each condition in blastema area measurement, n = 30 limbs for each condition in differentiation and digit outline quantification). **(G)** *Prrx1* HCR-FISH was performed on tissue sections at 5 dpa following local amputation of naïve limbs (no previous amputation) and primed limbs (previously amputated on the contralateral side 7 days earlier). **(H)** Quantification of *Prrx1* mean fluorescence intensity across entire tissue sections of naïve and primed blastemas (n = 8 animals for each group). **(I)** EdU and DAPI staining of intact control limbs (left) and limbs contralateral to amputation (right) harvested 6 weeks after EdU administration. **(J)** Quantification of percent EdU positive nuclei of intact and contralateral limbs in **(I),** (n = 15 animals for intact and n = 12 animals for contralateral group). **(K)** Representative images of systemically-activated and naïve limbs amputated 28 days post-contralateral amputation (ventral view, 7-21 dpa; dorsal view, 27 dpa). **(L-M)** Quantification of blastema area at 7 dpa **(L)** and number of digit outlines at 27 dpa **(M)** (n = 19 animals for control, n = 20 animals for activated for blastema area measurement, n = 38 limbs for control

and n = 40 limbs for systemically-activated animals in digit outline quantification). All data shown as mean ± SD. Statistical significance was determined using unpaired two-tailed Welch's t-test in **(D)**, **(H)**, **(J)** and **(L)**; and Fisher's exact test in **(E)**, and Fisher's exact test with Freeman-Halton extension in **(F)** and **(M).** Scale bars, 2 mm in **(C)** and **(K)**; 500 μm in **(G)** and **(I).** dpa, days post-amputation. EdU, 5-ethynyl-2′-deoxyuridine.

Figure 2. PNS at both amputation site and responding site are required for systemic activation. (A-E) Nerve bundles innervating limbs contralateral to unilateral amputations were transected or sham-operated, and animals were assayed for systemic activation. Animals receiving unilateral denervations or sham-operations with no amputations were used as controls. **(A)** EdU and DAPI staining of intact and contralateral limb tissue sections of denervated and sham-operated animals in the intact state or at 14 days post-amputation. **(B)** Quantification of percent EdU positive nuclei in denervated and sham-operated at 14 dpa. **(C-E)** Breakdown of tissue types represented in **(B)**. **(C)** Epidermis. **(D)** Skeletal elements. **(E)** Internal, non-skeletal tissues. (n = 11 animals for sham, n = 10 animals for denervated, n = 13 animals for sham amputated and denervated amputated, **(F-G)** Nerve bundles were transected or sham-operated in limbs that were immediately amputated thereafter. **(F)** EdU and DAPI staining of intact and contralateral limb tissue sections of denervated and sham-operated animals in the intact state or at 14 days post-amputation. **(G)** Quantification of percent EdU positive nuclei in denervated and sham-operated at 14 dpa (n = 18 animals for sham, n = 16 for sham amputated, n = 11 for denervated, and n = 12 for denervated amputated). **(H-I)** Differential gene expression analysis identifies transcripts that are enriched in nerve ends of contralateral limbs with nerve transections ("den") or sham operations ("sham") **(H)** and responding tissues **(I)**. All data shown as mean ± SD. Statistical significance was determined using unpaired two-tailed Welch's t-tests with Bonferroni-Dunn correction in **(B)**, **(C)**, **(D)**, **(E)** and **(G)**. Scale bars, 500 μm in **(A)** and **(F)**. den, denervated. int, intact. contra, contralateral. EdU, 5-ethynyl-2′-deoxyuridine. See also **Table S1**.

Figure 3. α-Adrenergic signaling is required for systemic activation and priming. (A-B) Plasma levels of **(A)** noradrenaline and **(B)** adrenaline at homeostasis and 4 hours post-amputation, as determined by ELISA. **(C)** EdU and DAPI staining of regenerating blastemas from animals treated with yohimbine or vehicle control, harvested at 12 days post-amputation. **(D)** Quantification of percent EdU positive nuclei in blastemas in **(C)** (n = 20 animals for vehicle, n = 13 animals for yohimbine). **(E)** EdU and DAPI staining of limbs contralateral to unilateral amputations treated with yohimbine or vehicle control, harvested at 7 days post-amputation. **(F)** Quantification of percent EdU positive nuclei in contralateral limbs in **(E)** (n = 15 animals for each group). **(G)** Experimental design. Animals were treated with chemical agonists or antagonists (treatment) or vehicle solution by daily injections or water treatments starting from 2-3 days before to 7 days post unilateral amputations. The treatments were then ceased, and the uninjured contralateral limbs were unilaterally amputated. The regeneration rates of the second set of amputations were compared between treatment groups. **(H)** Representative images of regenerating contralateral limbs of yohimbine and vehicle solution-treated animals (ventral view, 5-25 dpa; dorsal view, 32 dpa). **(I)** Quantification of blastema area at 14 days post-amputation (n=15 animals for each condition). **(J)** Quantification of the number of digit outlines at 25 days post-amputation (n = 30 limbs for each condition). **(K)** Representative images of regenerating contralateral limbs of clonidine and vehicle solution-treated animals (ventral view, 7-23 dpa; dorsal view, 33 dpa). **(L)** Quantification of blastema area at 7 days post-amputation. (n = 20 animals for vehicle and n = 18 animals for clonidine). **(M)** Quantification of the number of digit outlines at 23 days post-amputation (n = 40 limbs for vehicle and n = 35 limbs for clonidine). The same group of vehicle control animals was used in Figure 6S (H-J). **(N-P)** Animals were treated with beta-adrenergic receptor antagonist propranolol starting from 2 days before

to 7 days post unilateral amputations. **(N)** EdU and DAPI staining of blastemas and limbs contralateral to unilateral amputations treated with propranolol or vehicle control, harvested at 7 days post-amputation. **(O)** Quantification of percent EdU positive nuclei within the blastema area of the initially-amputated limbs (n = 15 animals for vehicle and n = 10 for propranolol). **(P)** Quantification of percent EdU positive nuclei within contralateral limbs at 7 dpa (n = 15 animals for vehicle and n = 10 for propranolol). **(Q-T)** Animals were treated with Adra2a agonist clonidine or vehicle solution starting from 2 days before to 7 days post unilateral amputations. **(Q)** Representative images of regenerating limbs at 7 days post-amputation. **(R)** Quantification of blastema area at 7 dpa (n = 25 animals for vehicle and n = 20 animals for clonidine). **(S)** Representative images of EdU staining of regenerating limbs harvested at 7 days post-amputation. **(T)** Quantification of percent EdU positive nuclei within the blastema area (n = 15 animals for vehicle and n = 14 for clonidine). All data shown as mean ± SD. Statistical significance was determined using paired two-tailed Welch's t-tests in **(A)** and **(B)**; unpaired two-tailed Welch's t-tests in **(D)**, **(F)**, **(I)**, **(O)**, **(P), (R)** and **(T)**; Welch's ANOVA with Dunnett's T3 correction in **(L)**; Fisher's exact test with Freeman-Halton extension in **(J)** and **(M)**. Scale bars, 500 μm in **(C), (E), (N)** and **(S)**; 2 mm in **(H), (K)** and **(Q)**. hpa, hours post-amputation. dpa, days post-amputation. EdU, 5-ethynyl-2′-deoxyuridine. YOH, yohimbine. See also **Figure S1.**

Figure 4. Systemically-activated cells represent the same broad cell types as cells proliferating during homeostasis. (A) Experimental design to identify systemically activated cells and compare to proliferating cells during homeostasis. Dividing (4C) cells of systemically-activated and naïve, control limbs were isolated by sorting dissociated cells according to their DNA content. **(B)** Representative FACS distribution following Hoechst stain of homeostatic and systemically-activated limb cell samples. **(C)** UMAP plot of 4C cells collected from homeostatic control limbs (n = 4) and systemically-activated limbs (n = 4). **(D)** UMAP plot of 4C cells with cells harvested from the homeostatic limb in blue and systemically-activated limb in red. **(E)** Heat map depicting statistically significant differential gene expression between 4C cells in homeostatic versus activated samples. Only cell types with differential gene expression are shown. **(F)** Dot plot showing the relative frequency of expression (dot size) and expression level (color) for differentially expressed genes across the eight fibroblast cell populations in homeostatic (H) versus activated (A) samples. **(G-H)** Mapping scores of axolotl **(G)** fibroblasts and **(H)** epidermal cells isolated from homeostatic and systemically-activated limbs to reindeer skin cells isolated from antler and back at homeostasis and post-injury. **(I)** UMAP plot of 2C cells collected from homeostatic control limbs (n = 3) and systemically-activated limbs (n = 4). **(J)** UMAP plot of 2C cells with cells harvested from the homeostatic limb in blue and systemically-activated limb in red. **(K)** Heat map depicting statistically significant differential gene expression between 2C cells in homeostatic versus activated samples. Only cell types with differential gene expression are shown. See also **Figure S2** and **S3, Table S2, S3, S4** and **S5.**

Figure 5. Systemically activated cells are epigenetically unique while also sharing some chromatin accessibility signatures with proliferating homeostatic and blastema cells. (A) Venn diagram illustrating significantly enriched predicted transcription factor binding motifs within open chromatin of each of the three conditions sampled, 4C cells from homeostatic limbs, 4C cells from regenerating limbs (blastema cells), 4C systemically-activated cells. Representative transcription factors are noted. **(B)** Expression of genes with putative p53 binding sites in 4C fibroblast populations **(C)** Luciferase activity assay in homeostatic and systemically-activated limbs. Firefly luciferase vector with p53 binding sites was electroporated alongside a *Renilla* luciferase control vector into right limbs of axolotls, immediately followed by amputation of the left limbs for the activated group. At 7 dpa, relative firefly luciferase activity

was determined by normalizing to *Renilla* luciferase activity. Statistical significance was determined using unpaired, two-tailed Welch's t-test in **(C)**. See also **Figure S4** and **S5,** and **Table S6**.

Figure 6. Main findings and implications of the study. (A) Systemic stem cell activation following amputation promotes faster regeneration. Systemic activation is driven by nerves and requires adrenergic signaling. **(B)** A two-step model for blastema cell specification. In step 1, some cells (green nuclei) from a field of possible progenitor cells re-enter the cell cycle (activation) and begin to proliferate in response to amputation. We postulate this step is systemic, occurring throughout the body. In step 2, some subset of activated progenitor cells later converts to the blastema cell state (blue cells). We postulate this step is local to the site of amputation. The subsequent migration of blastema cells to the distal-most tip of the stump creates a visible blastema (yellow).

STAR Methods

RESOURCE AVAILABILITY

Lead contact

Further information and requests for resources and reagents should be directed to and will be fulfilled by the lead contact, Jessica Whited (jessica_whited@harvard.edu).

Materials availability

This study did not generate new unique reagents.

Data and code availability

- All bulk RNA-sequencing data sets generated during this study are available at Gene Expression Omnibus (GEO), accession number GSE192477.
- All single-cell RNA-sequencing datasets generated in this study are available at Gene Expression Omnibus (GEO), accession numbers GSE232083 (4C) and GSE232082 (2C).
- All bulk ATAC-sequencing datasets generated in this study are available at Gene Expression Omnibus (GEO), accession number GSE232080.
- All original code has been deposited at Zenodo and is publicly available as of the date of publication. The DOI is listed in the key resources table.
- Any additional information required to reanalyze the data reported in this paper is available from the lead contact upon request.

EXPERIMENTAL MODEL AND SUBJECT DETAILS

Animals

All animal experimentation was approved by and conducted in accordance with Harvard University's Institutional Animal Care and Use Committee. Leucistic axolotls were used for all animal experiments except RNA sequencing and maintained as previously described.[5] For RNA sequencing, *βIIItub:GAP43-EGFP* transgenic animals were used.[94] Animals in all experiments were both age and size matched. Animals were anesthetized in 0.1% (w/v) tricaine prior to all procedures involving amputation, denervation, or injection. After all surgical procedures, axolotls were allowed to recover overnight in 0.5% (w/v) sulfamerazine. All limb amputations were performed at the mid-stylopod and the bone was then trimmed back from the amputation plane. For forelimb denervations the brachial plexus nerves were

transected as described previously,[95] and for hindlimb denervations the sciatic nerves were transected as described[96]. Sham operations as controls for denervations were performed by anesthetizing animals and cutting the skin open with sterile scissors, locating the nerve bundles with closed sterile forceps, but not cutting the nerves.

METHOD DETAILS

Denervations and amputations

Animals in all experiments were both age and size matched. Animals were anesthetized in 0.1% (w/v) tricaine prior to all procedures involving amputation, denervation, or injection. After all surgical procedures, axolotls were allowed to recover overnight in 0.5% (w/v) sulfamerazine. All limb amputations were performed at the mid-stylopod and the bone was then trimmed back from the amputation plane. For forelimb denervations the brachial plexus nerves were transected according to Schotté *et al.* [95] and for hindlimb denervations the sciatic nerves were transected according to Kropf *et al.* [96] Sham operations as controls for denervations were performed by anesthetizing animals and cutting the skin open with sterile scissors, locating the nerve bundles with closed sterile forceps, but not cutting the nerves.

Drug treatments and EdU incorporation

Rapamycin was dissolved into a 25 mg/mL stock solution in ethanol. Rapamycin treatments were delivered via both water treatments at a concentration of 1 μM for 16 days with water changed daily, and through daily intraperitoneal injections at a concentration of 5 mg/kg/day for 16 days, both starting two days before amputation. All intraperitoneal injections were administered at a volume of 20 μL/g in a vehicle solution comprised of APBS with 5% Tween80, 5% PEG-400. All stock solutions were frozen at −80 °C in 1-mL aliquots. Yohimbine (Y3125, Sigma-Aldrich) was dissolved into a 10 mg/mL stock solution with sterilized water. Yohimbine was administered daily at a dose of 1mg/kg for 14 days via intraperitoneal injection. A stock solution of IWR-1 (I0161, Sigma-Aldrich) was created by dissolving 5mg/mL in DMSO. IWR-1 was delivered daily at a dose of 10mg/kg/day for 9 days via intraperitoneal injection. A stock solution of NVP-ADW742 (5247, Tocris) was created by dissolving 2mg/mL in DMSO. NVP-ADW742 was injected daily at a dose of 10mg/kg/day for 14 days. Clonidine (C7897, Sigma-Aldrich) was dissolved in water at 7.5 mM stock concentration and was delivered via water treatments at 30 μM. A stock solution of propranolol (P0884, Sigma-Aldrich) was created by dissolving 100 mM in water. Propranolol was delivered via water treatments at 5 μM. AS1842856 (S8222, Selleck Chemicals) was dissolved in DMSO at a stock concentration of 12.5 mM and was delivered via intraperitoneal injections at a concentration of 10 mg/kg/day for 12 days. 5-ethynyl-2′-deoxyuridine (EdU) was purchased from ThermoFisher and stock solutions were created by dissolving the powder in dimethyl sulfoxide as instructed by the manufacturer. Following anesthetization, axolotls were administered 20 μL/g of 400 μM EdU in 0.7X PBS via intraperitoneal injection 18 hours before tissue harvest.

Skeletal and tissue preparations

For tissue sections, tissue samples were fixed in 4% paraformaldehyde post-collection in DEPC-treated PBS overnight at 4°C. Tissues were then cryopreserved in a sucrose gradient following a wash in DEPC-PBS and incubated in 30% sucrose/DEPC-PBS at 4°C overnight. Tissues were then embedded and frozen on dry ice in Tissue-Tek O.C.T. Compound (Sakura) and stored at −80°C. All blocks were sectioned at 16 μm thickness using a Leica CM 1950 cryotome and sections were stored at −80°C until use.

785 For skeletal preparations, post-collection, limbs were incubated overnight in 95% ethanol at room
786 temperature and then incubated in 100% acetone under the same conditions. Skeletal elements were
787 visualized with Alcian blue and Alizarin red S stains followed by a clearing of non-skeletal tissue with
788 potassium hydroxide.
789
790 **Immunofluorescence and HCR-FISH**
791 Sections were rehydrated with PBS and then permeabilized with 0.5% Triton-X-100 PBS. Post-
792 permeabilization, slides were rinsed twice with PBS and EdU visualization was performed via sulfo-
793 cyanine 3 azide (Lumiprobe). Post-EdU visualization slides were washed twice with PBS. Staining and
794 labeling with any additional antibodies was conducted post-EdU labeling. Primary antibodies used were
795 rabbit anti-phospho-S6 ribosomal protein (Ser235/236, 1:200; Cell Signaling 4858), mouse anti-NeuN
796 (1:200, Abcam ab104224). Secondary antibodies used were Cy3-goat anti-mouse (1:250, Jackson
797 ImmunoResearch 115-165-146), Alexa Fluor 488-Goat Anti-Rabbit (1:250, Jackson ImmunoResearch,
798 111-545-003) and Cy3-goat anti-rabbit (1:250, Jackson ImmunoResearch 111-165-003).
799
800 Sections stained with all antibodies were blocked with 10% serum from the host species of the secondary
801 antibody in 0.1% Triton-X-100 in PBS. Primary and secondary antibodies were diluted in in 2% BSA,
802 0.1% Triton-X-100 in PBS. Sections labeled with anti-pS6 and NeuN underwent an antigen retrieval step
803 after permeabilization, in which slides were boiled in 0.1 M sodium citrate (pH 6.0) and then rinsed once
804 in PBS, before EdU was visualized, followed by blocking and primary antibody incubation. All slides were
805 incubated with DAPI (Sigma D9542) before cover slipping. HCR-FISH was performed as described
806 previously.[97]
807
808 **Plasma isolation and ELISA**
809 Blood was collected from axolotls as described previously.[98] Efferent blood vessels were exposed by
810 placing the animals on its back. Winged infusion sets were used to collect the blood. Whole blood was
811 placed into EDTA coated tubes and spun down. The supernatant fraction (plasma) was used for
812 downstream analysis. Animals were allowed to recover overnight in fresh axolotl water. Epinephrine and
813 norepinephrine ELISAs were performed using Abnova ELISA kit KA1877.
814
815 **Luciferase Reporter Assay**
816 The vectors used for luciferase assay (PG13-luc (wt p53 binding sites) (Addgene #16442),
817 pGL4.73[*hRluc/SV40*] (Promega E6911), and pCAG-tdTomato to assess electroporation efficiency) were
818 diluted to a final concentration of 250 ng/μL in 0.7X PBS. Fast Green dye was added to aid in
819 visualization. The right intact limbs were each injected with 10 μL of the vector solution. For vector
820 delivery, animals were immersed in 1X PBS and electroporated using NepaGene Super Electroporator
821 NEPA21 Type II electroporator. The poring pulse was 3 pulses at 150 Volts with a pulse length of 5
822 milliseconds, a pulse interval of 10 milliseconds, a decay rate of 0 %, and a positive (+) polarity. The
823 transfer pulse was 5 pulses at 50 Volts with a pulse length of 50 milliseconds, a pulse interval of 950
824 milliseconds, a decay rate of 0 %, and a positive (+) polarity.
825
826 Immediately following electroporation, the left limbs of the systemically-activated group were amputated
827 proximally. Seven days post-electroporation, homeostatic and systemically activated limbs were
828 harvested, selecting tissues with positive tdTomato signal. Tissues were lysed in Dual-Glo Luciferase
829 Assay Reagent from the Dual-Glo Luciferase Assay System (Promega E2940), and debris was cleared
830 via centrifugation. The luciferase assay was then performed in a 96-well plate format according to the

manufacturer's instructions. The activity of firefly luciferase was normalized to the activity of the internal *Renilla* luciferase activity.

Imaging and quantification

Imaging was performed on a Zeiss Axio Scan.Z1 automated slide scanner, Leica M165 FC equipped with Leica DFC310 FX camera, and a Nikon Eclipse Ni microscope with a DS-Ri2 camera. Quantification of all images was conducted blindly. For imaging of homeostatic (intact), contralateral or regenerating limbs, representative sections displaying all non-epidermal tissue types were selected. For the tissue type analysis of EdU+ nuclei, tissues were classified as epidermis, "skeletal elements" (bone, cartilage), and "soft tissues" (muscle, joint, tendon, ligaments, dermis, vasculature, and nerves) based on nuclear morphology and location as previously described (Whited et al, 2013). All cell counts were conducted utilizing CellProfiler.[99] Measurements of blastema area were performed using Fiji.[100] For *Prrx1* HCR signal quantifications, the wound epidermis was first masked from each image. *Prrx1* fluorescence intensity was normalized to the area of the blastema as measured by the DAPI signal.

Bulk RNA isolation, sequencing, and computational analyses

βIIItub:GAP43-EGFP transgenic animals were used for RNA sequencing experiments to allow for easily identifiable collections of tissues.[94] RNA was extracted from tissue samples ("nerve" derived from nerve bundles in the limb without cell bodies; "surrounding tissues" derived from all other limb tissues minus the nerve) with Trizol (15596018, Ambion) and chloroform (288306, Sigma Aldrich). RNA was then isolated from tissue samples using a Zymo Clean Up and Concentrator kit (R1013). RNA samples were processed at the Bauer Core Facility at Harvard University using the Illumina NextSeq 500. Paired End reads were demultiplexed with bcl2fastq2 v2.2.

Cell dissociation, FACS isolation, and single-cell RNA-sequencing

To isolate single cells, 12-16 homeostatic or systemically-activated limbs at 14 days post-amputation were pooled for each biological replicate and dissociated in 4 ml of dissociation buffer (100 mg/ml liberase diluted in 0.7X PBS with 0.5 U/ml DNase I) for 30 min at room temperature with gentle mixing. Suspensions were filtered through 70 mm strainers to remove cell clumps and debris, and strainers were washed with 1 ml of 0.7X PBS. Cells were spun down at 300 g at room temperature and resuspended in 1 ml of 0.7X PBS-0.04% BSA. Cells were then stained with 1 mg/mL Hoecsht, calcein AM, and propidium iodide for isolation of alive, dividing (4C) and non-dividing (2C) cells by fluorescence activated cell sorting. The purified cells were then sequenced at the Bauer Core Facility at Harvard University using an Illumina NovaSeq 6000 [https://www.illumina.com]. Paired end reads were demultiplexed with bcl2fastq2 (V2.2.1) (RRRID:SCR_015058).

ATAC-seq Library Prep and Sequencing

Ten thousand sorted 4C cells from homeostatic, systemically-activated, and regenerating limbs were resuspended in 5 µL PBS. 42.5 µL of transposition buffer (38.8 mM tris-acetate, 77.6 mM potassium acetate, 11.8 mM magnesium acetate, 0.12% NP-40, 18.8% DMF, 0.47% protease inhibitor cocktail) was added to the cells, mixed, and incubated 10 min at room temperature. 2.5 µL of pre-loaded Tn5 (Diagenode cat# C01070012) was added to the reaction mixture. The transposition reaction was carried out at 37°C for 30 min with shaking at 300 rpm. Following transposition, the samples were purified through Direct-zol RNA MiniPrep kit (Zymo Research cat# R2050). Purified library fragments were amplified with custom primers 1 and 2 using the following conditions: 72°C for 5 min; 98°C for 30 s; and thermocycling at 98°C for 10 s, 72°C for 30 s and 72°C for 1 min. The libraries were amplified for five cycles. Soon after, 5 µL aliquot of the PCR reaction was added

878 with 10 µL of the PCR cocktail with SYBR Green (0.6Xfinal concentration). 20 cycles of PCR was
879 performed to determine the additional number of cycles needed for the remaining 45 µL reaction. The
880 libraries were purified using Direct-zol RNA MiniPrep kit. Purified libraries were sequenced at The Bauer
881 Core Facility at Harvard University using an Illumina NovaSeq 6000 [https://www.illumina.com]. Paired
882 End reads were demultiplexed with bcl2fastq2 (V2.2.1) (RRID: SCR_015058).
883
884 **QUANTIFICATION AND STATISTICAL ANALYSIS**
885
886 **Bulk RNA-seq dataset processing**
887 The reads were trimmed for quality and adapters with Trimmomatic v0.39[101] with the following
888 parameters: LEADING:3 TRAILING:3 SLIDINGWINDOW:4:15 MINLEN:36. An index of the previously
889 published axolotl transcriptome[5] was created using Kallisto v0.45.1.[102] Sequence based bias correction
890 was performed using Kallisto with 200 bootstraps across 20 threads. The transcript-level abundances
891 from Kallisto were summarized and imported into R as a matrix of counts using tximport v1.0.3.[103]
892 Differentially expressed genes were determined by estimating fold change and dispersion using
893 DESeq2.[104] Genes were considered significant if they had a logarithmic fold change greater than 1.5 and
894 adjusted p value of 5%. These significant genes were visualized using pheatmap v1.0.12.[105] Pathway
895 analysis was performed in R using pathfinder.[106]
896
897 **Minigenome**
898 A custom reference "minigenome" was created by first performing in silico normalization on the
899 sequenced reads by sample with Trinity (V2.12.0)[107] with the following parameters: --CPU 10 --
900 max_memory 50G --no_run_inchworm --min_kmer_cov 2 --trimmomatic --seqType fq, before assembling
901 them with parameters: --CPU 10 --max_memory 50G --min_kmer_cov 3 --seqType fa --
902 no_normalize_reads. This transcriptome was then aligned to the entire axolotl genome (V6.0.0)
903 [https://www.axolotl-omics.org/assemblies][108] using minimap2 (V2.24)][109] and the parameters -ax splice --
904 secondary=no -O6,24 -B4 -L -t 20 -cs -ub -G 100000 to create genome intervals of the genes present in
905 the transcriptome. The intervals were converted from the original SAMtools (V1.15.1)[110] format to BED
906 using BEDOPS (V2.4.25).[111] Finally, the minigenome and annotation was created from the intervals
907 using ShrinkGenome [https://github.com/brianjohnhaas/ShrinkGenome]. The complete axolotl
908 mitochondrial genome [https://www.ncbi.nlm.nih.gov/nuccore/NC_005797][112] was then appended to this
909 minigenome. We prevented competitive alignments to mitochondrial contributors downstream by
910 masking their genomic loci using the maskFastaFromBed function from BEDTools (V2.30.0).[113]
911
912 **Single-cell RNA-sequencing read quantification**
913 We used Kallisto (V0.48.0)[102] to create an index, as well as pseudoalign the RNA-seq data before
914 creating BUS [114] files by biological replicate. The BUS files were sorted and converted into text using
915 bustools (V0.41.0)[115] using default parameters before converting the BUS files into sparse matrices of
916 gene by cell data in R using BUSpaRse (V1.9.0).[116] The gene by cell sparse matrices were converted
917 into Seurat[117] objects in R, filtering out cells with less than 200 transcripts as well as any feature that was
918 in less than 3 cells, before merging the sample replicates into either homeostatic samples or systemically
919 activated samples, which were merged into a single data structure, while maintaining their original
920 metadata. For QC, cells were scored for their complexity with the following formula cell complexity =
921 $\log_{10}$(# of genes in cell) / $\log_{10}$(# of UMI in cell). If a cell had less than 1,000 UMI while also both
922 expressing less than 350 features and a cell complexity score less than 0.75 it was not considered a
923 candidate for analysis and removed from the dataset.
924

925 **Cell clustering and visualization**
926 Clustering the cells was performed with Seurat (V4.1.0). Default parameters were used in the
927 FindVariableFeatures function of Seurat to determine the number of principal components. We used a
928 resolution of 1.0 to cluster the cells with 17 dimensions. We generated markers for the clusters and found
929 that one of the clusters consisted primarily of mitochondrial markers. This cluster was eliminated and the
930 cell clustering pipeline was repeated. We performed homotypic doublet proportion estimation to predict
931 and remove doublets using DoubletFinder (V2.0.3)[117] as described at [https://github.com/chris-mcginnis-
932 ucsf/DoubletFinder]. The cell clusters were visualized with the reduction method UMAP. Clusters were
933 identified by unique markers in each cluster.
934
935 **Differential gene expression analysis for single-cell RNA sequencing**
936 We searched for differentially expressed genes between the homeostatic and systemically activated cells
937 using DESeq2 (V1.36.0).[104] The contrast in the results was configured by condition, where homeostatic
938 limb was the baseline and systemically activated limb was the contrasting condition. The results were
939 determined to be significant if the adjusted p-value was less than 0.1. Statistically significant results were
940 visualized with ggplot2 (V3.3.6).[118]
941
942 **CellChat analysis**
943 To obtain the information related to incoming and outgoing clusters ligand-receptors interactions, we used
944 the CellChat package[119] for 4C datasets using the previously generated Seurat objects. A custom axolotl
945 ligand-receptor reference was generated using the minigenome. The database included information on
946 ligands and receptors, and for orthologous gene repeats that have different positions in the genome and
947 different annotations, labeled as "Gene_ik", where k is the number of the repeats. The database was
948 reconstructed following the ligand-receptor pairs used for the mouse CellChat database with the gene
949 repeats included as separated ligand-receptor pairs (L1-R1, L1_i1_R1, etc.).
950 After generating the database, we followed the standard CellChat pipeline
951 [https://github.com/sqjin/CellChat/]. To avoid the projection reducing the dropout effects of signaling
952 genes, for possible zero expression of subunits of ligands/receptors, we used raw.use = FALSE setting in
953 computeCommunProb function. We also used population.size = TRUE parameter to consider the effect of
954 cell proportion in each cell group in the probability calculation. The chord diagrams were generated using
955 netVisual_aggregate() function.
956
957 **RNA Velocity**
958 Upon the clusters to states annotation, we utilized Cell ranger, samtools, velocyto, and scvelo packages
959 to perform the RNA Velocity analysis[120]. For the previously generated Cellranger output folder, we used
960 the samtools sort function in the samtools package (-t CB -O BAM) to create the
961 cellsorted_possorted_genome_bam.bam file from the possorted_genome_bam.bam file. The generated
962 file was used for making the .loom file upon utilizing the velocyto run10x function of the velocyto package,
963 using the minigenome. We then converted the .h5Seurat annotated objects to .h5ad objects to transfer
964 them from R to the Python environment. We used the scvelo package[121] for the RNA Velocity analysis.
965 We merged .loom files with the respective data files previously generated, processed, and annotated. The
966 following files were filtered and normalized. The first and second order moments (means and uncentered
967 variances) were computed among nearest neighbors in PCA space with the scvelo.pp.moments()
968 function. Then we estimated velocity (scvelo.tl.velocity()), built the velocity_graph
969 (scvelo.tl.velocity_graph()) and projected the velocities using scvelo.pl.velocity_embedding_stream() and
970 scvelo.pl.velocity_embedding_grid() on UMAP (basis = 'umap') embedding. With that, we quantified
971 pseudotime, latent time, and built the latent-time-based heatmaps with gene RNA abundance analysis.

Chunked Genome

A custom "chunked genome" was needed for compatibility with tools used to process the alignments. We broke the large chromosomes of the axolotl genome (v6.0.0) [https://www.axolotl-omics.org/assemblies][112] into chunks smaller than 500M using ChunkGenome [https://github.com/brianjohnhaas/ChunkGenome]. ChunkGenome was also used to create a new feature coordinates from the original GTF. The complete axolotl mitochondrial genome [https://www.ncbi.nlm.nih.gov/nuccore/NC_005797][112] was appended to this chunked genome. We prevented competitive alignments to mitochondrial contributors downstream by masking their genomic loci using the maskFastaFromBed function from BEDTools (v2.30.0) [https://github.com/arq5x/bedtools2].[113]

ATAC-seq read processing

We aligned sequencing reads to the reference genome using Bowtie2 (v2.3.2)[122] with parameters optimized for local alignment (--no-mixed), high sensitivity (-X 2000), gapped alignment (--dovetail), and exclusion of discordant read pairs (--no-discordant). Alignments were sorted and indexed throughout the analysis using Samtools (v1.10)[123] for efficient retrieval. Mitochondrial reads were filtered out using grep to focus on nuclear DNA.Low-quality alignments (MAPQ score < 30) were removed using Samtools. PCR and optical duplicates were identified and removed with Picard MarkDuplicates[124] [https://broadinstitute.github.io/picard/] assuming sorted alignments (ASSUME_SORTED=true) and removing all identified duplicates (REMOVE_DUPLICATES=true). Generation of bigwig Coverage Tracks was performed with deepTools bamCoverage[125]. We specified --outFileFormat=bigwig for bigWig output, --normalizeUsing CPM for counts per million normalization, and --binSize 20 for a bin size of 20 base pairs.

ATAC-seq peak calling

Open chromatin regions were identified using MACS2 (v2.2.9.1)[126] (https://github.com/macs3-project/MACS). We employed two peak calling strategies: consensus peaks, generated by analyzing all replicates/samples together, and condition-specific peaks.

Annotating and visualizing the ATAC data

We employed ChIPseeker (v1.32.1)[127] to annotate the peaks. Subread featurecount (v1.32.1)[128] was used to create a gene by peak count matrix. Differential accessibility was observed using DESeq2.[104] To visualize normalized counts and sample clustering, we used Pheatmap (v1.9.12) (10.32614/CRAN.package.pheatmap) [129] and pcaExplorer (v2.22.0)[130], respectively. Motif discovery and enrichment analysis were performed using HOMER (v4.11).[131] Briefly, motifs from HOMER analysis were read into MATLAB and significant motifs identified in each replicate for each condition. Replicates with number of enriched motifs significantly lower than in other replicates for the same condition were discarded in further analyses. 4C single-cell gene expression linked to discovered motifs was visualized with Seurat's DotPlot function.[132] We preprocessed the 4C data using Seurat's AggregateExpression function with log normalization and scaling. Heatmaps of the aggregated 4C single cell counts were generated with pheatmap (10.32614/CRAN.package.pheatmap)[129]. Finally, pathway enrichment analysis of the transcription factors was performed using Panther[133] and visualized with ggplot2.[134]

Mapping cell manifolds across axolotl and reindeer

We began by mapping the axolotl and custom reindeer transcriptome (Sinha, 2022) using reciprocal BLAST[135] with the following parameters: -evalue 1e-6 and -max_hsps 1.Fibroblast and epidermal populations from axolotl 4C and 2C conditions, as well as previously published reindeer single-cell data[33] were subsetted in Seurat. The single-cell data from both species were converted into an unprocessed state while retaining cell metadata. We employed the self-assembling manifold (SAM) algorithm as described by Tarashansky[136] and the SAMap project GitHub [https://github.com/atarashansky/SAMap], to compare cells between species. Briefly, we constructed manifolds for each dataset separately, before calculating new neighborhoods for all cells across the two species, and finally combined the manifolds into a single manifold. This was done separately for cells from different stages of the cell cycle, specifically 2C and 4C cells. Lowly alignment scores (< 0.05) produced by SAMap were filtered out before plotting with Heatmapply (v1.5.0)[137].

SUPPLEMENTAL FIGURE LEGENDS

Figure S1. Activation of α-adrenergic signaling is not sufficient for systemic activation (Related to Figure 3). **(A)** Cartoon depicting nerves innervating the axolotl limb in the naïve state (left) and the sham-operation procedure described in Figure 2 (right). **(B-C)** Dot plots showing the relative frequency of expression (dot size) and expression level (color) of **(B)** adrenergic receptors and **(C)** genes involved in adrenaline/noradrenaline biosynthesis pathway in axolotl dorsal root ganglia (re-analyzing data from Bhuiyan *et al*. 2024[19]). **(D)** Representative images of EdU and DAPI stained intact limbs harvested from animals treated with Adra2a agonist clonidine or vehicle solution for 9 days. **(E)** Quantification of percent EdU positive nuclei in the intact limb (n = 14 animals for vehicle and n = 12 for clonidine). **(F-G)** Animals treated with Adra2a agonist clonidine or vehicle solution were unilaterally denervated followed by proximal amputations. **(F)** Representative images of EdU and DAPI stained limbs contralateral to denervated and amputated limbs, harvested at 14 days post-amputation. **(G)** Quantification of percent EdU positive nuclei of contralateral limbs in **(F)** (n = 19 animals for vehicle and n = 17 for clonidine). **(H-I)** Animals treated with Adra2a agonist clonidine or vehicle solution were unilaterally denervated on one side, followed by unilateral proximal amputations of the innervated limbs. **(H)** Representative images of EdU and DAPI stained limbs, denervated and contralateral to unilateral amputations, harvested at 14 days post-amputation. **(I)** Quantification of percent EdU positive nuclei of denervated contralateral limbs in **(H)** (n = 17 animals for vehicle and n = 15 for clonidine). Statistical significance was determined using unpaired two-tailed Welch's t-test in **(E)**, **(G)** and **(I)**. Scale bars, 500 μm. EdU, 5-ethynyl-2′-deoxyuridine.

Figure S2. Marker genes used to identify clusters in single-cell RNA sequencing of 4C and 2C cells (Related to Figure 4). (A) Dot plots showing the relative frequency of expression (dot size) and expression level (color) of marker genes across all clusters of 4C cells. **(B)** Mapping scores of 2C and 4C axolotl fibroblast populations against reindeer antler and back skin cells pre- and post-injury. **(C)** Cell fate reconstruction analysis of 4C cells in homeostatic and systemically activated limbs. **(D)** Latent time-ordered heatmaps demonstrating variable genes across 4C fibroblast clusters. **(E)** Gene dynamics analysis shows the top 15 genes across the 4C cells with the most unique RNA abundance portraits. X-axis shows the spliced and the y-axis shows the unspliced transcripts for the gene, the steady state marked with the line. Each dot represents a single cell, with colors describing the clusters indicated on the right. **(F)** Dot plots showing the relative frequency of expression (dot size) and expression level (color) for marker genes across all clusters of 2C cells.

Figure S3. Adrenergic receptors expression in proliferating fibroblasts (Related to Figure 4). Dot plot showing the relative frequency of expression (dot size) and expression level (color) for adrenergic receptors across all clusters of 4C cells.

Figure S4. Expression levels of selected transcription factors with accessible binding sites in proliferating cells of homeostatic, regenerating, or systemically activated limbs (Related to Figure 5). Dot plots showing the relative frequency of expression (dot size) and expression level (color) of transcription factors across all cell populations of 4C cells in homeostatic (H) and activated (A) limbs.

Figure S5. Insulin/IGF signaling is required for systemic activation and limb regeneration (Related to Figure 5). (A) Select significant GO terms of genes with putative SMAD3 binding sites in 4C fibroblasts. **(B)** Dot plot showing the relative frequency of expression (dot size) and expression level (color) for Foxo transcription factors across fibroblast clusters of 4C cells in homeostatic (H) versus activated (A) limbs. **(C)** Representative images of regenerating limbs (ventral view) from animals treated with FOXO1 inhibitor AS1842856 or vehicle starting from 2 days before to 7 days post proximal forelimb amputations. **(D)** Quantification of blastema area at 10 dpa (n = 7 animals for vehicle and n = 5 for AS1842856 **(E-F)** Chord diagrams of CellChat analysis of Igf1r signaling **(E)** and insulin signaling **(F)** between 4C cell types identified by scRNA-seq in Figure 4. **(G)** EdU and DAPI staining of limbs contralateral to unilateral amputations treated with tankyrase inhibitor IWR-1, Igf1r inhibitor NVP-ADW742 or vehicle control, harvested at 7 days post-amputation. **(H)** Quantification of percent EdU positive nuclei of contralateral limbs in **(G)** (n = 11 animals for vehicle control, n = 14 animals for IWR-1 and NVP-ADW742). All data are shown as mean ± SD. Statistical significance was determined using unpaired, two-tailed Welch's t-test in **(D)** and Welch's ANOVA with Dunnett's T3 correction, W = 4.883 in **(H)**. Scale bars, 1 mm in **(C)** and 500 μm in **(G)**. NVP, NVP-ADW742. EdU, 5-ethynyl-2′-deoxyuridine. dpa, days post-amputation.

Figure S6. mTOR signaling is required for systemic activation and priming. (A) Chord diagrams of CellChat analysis of HGF signaling between cell types identified by scRNA-seq in Figure 4. **(B)** Regenerating limbs at 7 dpa treated with rapamycin or vehicle control. Arrowheads mark the amputation plane. **(C)** Blastema growth curves of rapamycin or vehicle-treated animals (n = 10 animals per group). Statistical significance was determined using unpaired two-tailed Welch's t-test with Holm-Šídák correction). **(D)** Representative skeletal preparations of regenerated limbs with Alcian blue and Alizarin red at 10 weeks post-amputation. **(E)** EdU and DAPI staining of rapamycin or vehicle-treated blastemas at 14 dpa. Arrowheads mark the amputation plane. **(F)** Quantification of percent EdU positive nuclei in **(E)**. **(G)** pS6 and EdU staining of intact (homeostatic) and contralateral limb tissue sections from animals treated with saline, vehicle, or rapamycin at 14 dpa. **(H)** Quantification EdU positive nuclei at 14 dpa (n = 12 limbs for intact saline, intact vehicle and intact rapamycin groups, n = 10 limbs for amputated saline and amputated vehicle, and n = 8 limbs for amputated rapamycin group). **(I)** Experimental design to test requirement for mTOR in priming. Animals were treated with rapamycin or vehicle solution by daily injections starting from 3 days before to 7 days post unilateral amputations. The treatments were then ceased, and the uninjured contralateral limbs were unilaterally amputated. The regeneration rates of the second set of amputations were compared between treatment groups. **(J)** Representative images of regenerating contralateral limbs of rapamycin and vehicle solution-treated animals. **(K)** Quantification of blastema area at 7 days post-amputation. **(L)** Quantification of the number of digit outlines at 23 days post-amputation (n=20 animals for vehicle and rapamycin; n = 40 limbs for vehicle and rapamycin for each condition in digit outline quantification). The same group of vehicle control animals were used in Figure 3 (K-M). **(M-N)** Animals fasting for four weeks were treated with mTORC1 inhibitor rapamycin or

vehicle control solution from 2 days before to 14 days post-unilateral amputations. **(M)** EdU and DAPI staining of limbs contralateral to unilateral amputations from animals treated with rapamycin or vehicle control, harvested at 14 dpa. **(N)** Quantification of percent EdU positive nuclei in **(M)**. **(O-P)** Animals fasting for four weeks were treated with ADRA2A inhibitor yohimbine or vehicle control from 2 days before to 7 days post-unilateral amputations. **(O)** EdU and DAPI staining of limbs contralateral to unilateral amputations from animals treated with yohimbine or vehicle control, harvested at 7 dpa. **(P)** Quantification of percent EdU positive nuclei in **(O)**. **(Q)** pS6, NeuN and EdU staining of dorsal root ganglia servicing homeostatic, amputated, and contralateral limbs at 7 days post-amputation (n = 19 for homeostatic, n = 15 for amputated and contralateral). **(R-S)** Quantification of percent EdU positive **(R)** and pS6, NeuN double positive **(S)** nuclei for DRGs in **(Q)**. All data shown as mean ± SD. Statistical significance was determined using unpaired two-tailed Welch's t-test with Holm-Šídák correction in **(C)**; unpaired two-tailed Welch's t-test in **(F)**, **(N)** and **(P)**; unpaired two-tailed Welch's t-test with Bonferroni-Dunn correction in **(H)**; two-tailed Welch's ANOVA with Dunnett's T3 correction for multiple hypothesis testing in **(K)**, **(R)** and **(S)**; and Fisher's exact test with Freeman-Halton extension in **(L)**. Scale bars, 0.5 mm in **(B)**; 500 μm in **(E)**, **(G), (M)** and **(O)**; 2 mm in **(H)**; and 100 μm in **(Q)**. rapa, rapamycin. Int, intact. contra, contralateral. dpa, days post-amputation. pS6, phospho-S6 ribosomal protein; NeuN, neuronal nuclei; EdU, 5-ethynyl-2′-deoxyuridine.

SUPPLEMENTAL EXCEL TABLE LEGENDS

Table S1. List of differentially expressed transcripts between sham-operated and denervated forelimbs contralateral to unilateral amputations (Related to Figure 2).

Table S2. List of transcripts expressed by each cluster of 4C cells in homeostatic and systemically-activated limbs (Related to Figure 4).

Table S3. Differentially expressed transcripts expressed by each cluster of 4C cells in homeostatic and systemically-activated limbs (Related to Figure 4).

Table S4. List of transcripts expressed by each cluster of 2C cells in homeostatic and systemically-activated limbs (Related to Figure 4).

Table S5. Differentially expressed transcripts expressed by each cluster of 2C cells in homeostatic and systemically-activated limbs (Related to Figure 4).

Table S6. List of accessible transcription factor binding motifs enriched across 4C cells of homeostatic, activated, and regenerating limbs. (Related to Figure 5).

References

1. Spallanzani, L. (1769 [Italian: 1768].). Reproductions of the legs in the aquatic salamander. In An Essay on Animal Reproductions [Prodromo di un opera da imprimersi sopra la riproduzioni anamali], (Becket and de Hondt), pp. 68-72.
2. Simon, A., and Tanaka, E.M. (2013). Limb regeneration. Wiley Interdiscip Rev Dev Biol *2*, 291-300. 10.1002/wdev.73.
3. Voss, S.R., Palumbo, A., Nagarajan, R., Gardiner, D.M., Muneoka, K., Stromberg, A.J., and Athippozhy, A.T. (2015). Gene expression during the first 28 days of axolotl limb regeneration I:

Experimental design and global analysis of gene expression. Regeneration (Oxford, England) *2*, 120-136. 10.1002/reg2.37.

4. Stewart, R., Rascon, C.A., Tian, S., Nie, J., Barry, C., Chu, L.F., Ardalani, H., Wagner, R.J., Probasco, M.D., Bolin, J.M., et al. (2013). Comparative RNA-seq analysis in the unsequenced axolotl: the oncogene burst highlights early gene expression in the blastema. PLoS computational biology *9*, e1002936. 10.1371/journal.pcbi.1002936.
5. Bryant, D.M., Johnson, K., DiTommaso, T., Tickle, T., Couger, M.B., Payzin-Dogru, D., Lee, T.J., Leigh, N.D., Kuo, T.H., Davis, F.G., et al. (2017). A Tissue-Mapped Axolotl De Novo Transcriptome Enables Identification of Limb Regeneration Factors. Cell reports *18*, 762-776. 10.1016/j.celrep.2016.12.063.
6. Gerber, T., Murawala, P., Knapp, D., Masselink, W., Schuez, M., Hermann, S., Gac-Santel, M., Nowoshilow, S., Kageyama, J., Khattak, S., et al. (2018). Single-cell analysis uncovers convergence of cell identities during axolotl limb regeneration. Science *362*. 10.1126/science.aaq0681.
7. Leigh, N.D., Dunlap, G.S., Johnson, K., Mariano, R., Oshiro, R., Wong, A.Y., Bryant, D.M., Miller, B.M., Ratner, A., Chen, A., et al. (2018). Transcriptomic landscape of the blastema niche in regenerating adult axolotl limbs at single-cell resolution. Nat Commun *9*, 5153. 10.1038/s41467-018-07604-0.
8. Sun, F., and Poss, K.D. (2023). Inter-organ communication during tissue regeneration. Development *150*. 10.1242/dev.202166.
9. Ricci, L., and Srivastava, M. (2018). Wound-induced cell proliferation during animal regeneration. Wiley Interdiscip Rev Dev Biol *7*, e321. 10.1002/wdev.321.
10. Wenemoser, D., and Reddien, P.W. (2010). Planarian regeneration involves distinct stem cell responses to wounds and tissue absence. Dev Biol *344*, 979-991. 10.1016/j.ydbio.2010.06.017.
11. Newmark, P.A., and Sanchez Alvarado, A. (2000). Bromodeoxyuridine specifically labels the regenerative stem cells of planarians. Dev Biol *220*, 142-153. 10.1006/dbio.2000.9645.
12. Salo, E., and Baguna, J. (1984). Regeneration and pattern formation in planarians. I. The pattern of mitosis in anterior and posterior regeneration in Dugesia (G) tigrina, and a new proposal for blastema formation. J Embryol Exp Morphol *83*, 63-80.
13. Johnson, K., Bateman, J., DiTommaso, T., Wong, A.Y., and Whited, J.L. (2018). Systemic cell cycle activation is induced following complex tissue injury in axolotl. Dev Biol *433*, 461-472. 10.1016/j.ydbio.2017.07.010.
14. Frobisch, N.B., Bickelmann, C., and Witzmann, F. (2014). Early evolution of limb regeneration in tetrapods: evidence from a 300-million-year-old amphibian. Proceedings. Biological sciences *281*, 20141550. 10.1098/rspb.2014.1550.
15. Moreno, G. (1989). Behavioral and Physiological Differentiation between the Color Morphs of the Salamander, Plethodon cinereus. Journal of Herpetology *23*, 335-341. 10.2307/1564043.
16. Verissimo, K.M., Perez, L.N., Dragalzew, A.C., Senevirathne, G., Darnet, S., Barroso Mendes, W.R., Ariel Dos Santos Neves, C., Monteiro Dos Santos, E., Nazare de Sousa Moraes, C., Elewa, A., et al. (2020). Salamander-like tail regeneration in the West African lungfish. Proc Biol Sci *287*, 20192939. 10.1098/rspb.2019.2939.
17. Group, I.S.A.S. (2020). Ambystoma mexicanum. The IUCN Red List of Threatened Species 2020: e.T1095A53947343.
18. Satoh, A., Gardiner, D.M., Bryant, S.V., and Endo, T. (2007). Nerve-induced ectopic limb blastemas in the Axolotl are equivalent to amputation-induced blastemas. Dev Biol *312*, 231-244. 10.1016/j.ydbio.2007.09.021.
19. Bhuiyan, S.A., Xu, M., Yang, L., Semizoglou, E., Bhatia, P., Pantaleo, K.I., Tochitsky, I., Jain, A., Erdogan, B., Blair, S., et al. (2024). Harmonized cross-species cell atlases of trigeminal and dorsal root ganglia. Science Advances *10*, eadj9173. doi:10.1126/sciadv.adj9173.
20. Rao, Y. (2019). The First Hormone: Adrenaline. Trends Endocrinol Metab *30*, 331-334. 10.1016/j.tem.2019.03.005.
21. Jabir, N.R., Firoz, C.K., Zughaibi, T.A., Alsaadi, M.A., Abuzenadah, A.M., Al-Asmari, A.I., Alsaieedi, A., Ahmed, B.A., Ramu, A.K., and Tabrez, S. (2022). A literature perspective on the pharmacological applications of yohimbine. Ann Med *54*, 2861-2875. 10.1080/07853890.2022.2131330.

22. Tam, S.W., Worcel, M., and Wyllie, M. (2001). Yohimbine: a clinical review. Pharmacol Ther *91*, 215-243. 10.1016/s0163-7258(01)00156-5.
23. Black, J.W., Crowther, A.F., Shanks, R.G., Smith, L.H., and Dornhorst, A.C. (1964). A New Adrenergic Betareceptor Antagonist. Lancet *1*, 1080-1081. 10.1016/s0140-6736(64)91275-9.
24. Muneoka, K., Holler-Dinsmore, G.V., and Bryant, S.V. (1985). A quantitative analysis of regeneration from chimaeric limb stumps in the axolotl. J Embryol Exp Morphol *90*, 1-12.
25. Muneoka, K., Fox, W.F., and Bryant, S.V. (1986). Cellular contribution from dermis and cartilage to the regenerating limb blastema in axolotls. Dev Biol *116*, 256-260.
26. Kragl, M., Knapp, D., Nacu, E., Khattak, S., Maden, M., Epperlein, H.H., and Tanaka, E.M. (2009). Cells keep a memory of their tissue origin during axolotl limb regeneration. Nature *460*, 60-65. 10.1038/nature08152.
27. McCusker, C.D., Diaz-Castillo, C., Sosnik, J., A, Q.P., and Gardiner, D.M. (2016). Cartilage and bone cells do not participate in skeletal regeneration in Ambystoma mexicanum limbs. Dev Biol *416*, 26-33. 10.1016/j.ydbio.2016.05.032.
28. Carver, E.A., Jiang, R., Lan, Y., Oram, K.F., and Gridley, T. (2001). The mouse snail gene encodes a key regulator of the epithelial-mesenchymal transition. Mol Cell Biol *21*, 8184-8188. 10.1128/MCB.21.23.8184-8188.2001.
29. Barbera, M.J., Puig, I., Dominguez, D., Julien-Grille, S., Guaita-Esteruelas, S., Peiro, S., Baulida, J., Franci, C., Dedhar, S., Larue, L., and Garcia de Herreros, A. (2004). Regulation of Snail transcription during epithelial to mesenchymal transition of tumor cells. Oncogene *23*, 7345-7354. 10.1038/sj.onc.1207990.
30. Lamouille, S., Xu, J., and Derynck, R. (2014). Molecular mechanisms of epithelial-mesenchymal transition. Nat Rev Mol Cell Biol *15*, 178-196. 10.1038/nrm3758.
31. Buckbinder, L., Talbott, R., Seizinger, B.R., and Kley, N. (1994). Gene regulation by temperature-sensitive p53 mutants: identification of p53 response genes. Proc Natl Acad Sci U S A *91*, 10640-10644. 10.1073/pnas.91.22.10640.
32. Haidurov, A., and Budanov, A.V. (2020). Sestrin family - the stem controlling healthy ageing. Mech Ageing Dev *192*, 111379. 10.1016/j.mad.2020.111379.
33. Sinha, S., Sparks, H.D., Labit, E., Robbins, H.N., Gowing, K., Jaffer, A., Kutluberk, E., Arora, R., Raredon, M.S.B., Cao, L., et al. (2022). Fibroblast inflammatory priming determines regenerative versus fibrotic skin repair in reindeer. Cell *185*, 4717-4736.e4725. 10.1016/j.cell.2022.11.004.
34. La Manno, G., Soldatov, R., Zeisel, A., Braun, E., Hochgerner, H., Petukhov, V., Lidschreiber, K., Kastriti, M.E., Lonnerberg, P., Furlan, A., et al. (2018). RNA velocity of single cells. Nature *560*, 494-498. 10.1038/s41586-018-0414-6.
35. Sun, F., Ou, J., Shoffner, A.R., Luan, Y., Yang, H., Song, L., Safi, A., Cao, J., Yue, F., Crawford, G.E., and Poss, K.D. (2022). Enhancer selection dictates gene expression responses in remote organs during tissue regeneration. Nat Cell Biol *24*, 685-696. 10.1038/s41556-022-00906-y.
36. Gardner, C.A., and Barald, K.F. (1992). Expression patterns of engrailed-like proteins in the chick embryo. Dev Dyn *193*, 370-388. 10.1002/aja.1001930410.
37. Loomis, C.A., Harris, E., Michaud, J., Wurst, W., Hanks, M., and Joyner, A.L. (1996). The mouse Engrailed-1 gene and ventral limb patterning. Nature *382*, 360-363. 10.1038/382360a0.
38. Tzchori, I., Day, T.F., Carolan, P.J., Zhao, Y., Wassif, C.A., Li, L., Lewandoski, M., Gorivodsky, M., Love, P.E., Porter, F.D., et al. (2009). LIM homeobox transcription factors integrate signaling events that control three-dimensional limb patterning and growth. Development *136*, 1375-1385. 10.1242/dev.026476.
39. Yang, Y., and Wilson, M.J. (2015). Lhx9 gene expression during early limb development in mice requires the FGF signalling pathway. Gene Expr Patterns *19*, 45-51. 10.1016/j.gep.2015.07.002.
40. Szeto, D.P., Rodriguez-Esteban, C., Ryan, A.K., O'Connell, S.M., Liu, F., Kioussi, C., Gleiberman, A.S., Izpisua-Belmonte, J.C., and Rosenfeld, M.G. (1999). Role of the Bicoid-related homeodomain factor Pitx1 in specifying hindlimb morphogenesis and pituitary development. Genes Dev *13*, 484-494. 10.1101/gad.13.4.484.
41. Logan, M., and Tabin, C.J. (1999). Role of Pitx1 upstream of Tbx4 in specification of hindlimb identity. Science *283*, 1736-1739. 10.1126/science.283.5408.1736.
42. Kruse, J.P., and Gu, W. (2008). SnapShot: p53 posttranslational modifications. Cell *133*, 930-930 e931. 10.1016/j.cell.2008.05.020.

1267 43. Yun, M.H., Gates, P.B., and Brockes, J.P. (2013). Regulation of p53 is critical for vertebrate limb
1268 regeneration. Proc Natl Acad Sci U S A *110*, 17392-17397. 10.1073/pnas.1310519110.
1269 44. el-Deiry, W.S., Tokino, T., Velculescu, V.E., Levy, D.B., Parsons, R., Trent, J.M., Lin, D., Mercer,
1270 W.E., Kinzler, K.W., and Vogelstein, B. (1993). WAF1, a potential mediator of p53 tumor
1271 suppression. Cell *75*, 817-825. 10.1016/0092-8674(93)90500-p.
1272 45. Denis, J.F., Sader, F., Gatien, S., Villiard, E., Philip, A., and Roy, S. (2016). Activation of Smad2
1273 but not Smad3 is required to mediate TGF-beta signaling during axolotl limb regeneration.
1274 Development *143*, 3481-3490. 10.1242/dev.131466.
1275 46. Furuyama, T., Yamashita, H., Kitayama, K., Higami, Y., Shimokawa, I., and Mori, N. (2002).
1276 Effects of aging and caloric restriction on the gene expression of Foxo1, 3, and 4 (FKHR,
1277 FKHRL1, and AFX) in the rat skeletal muscles. Microsc Res Tech *59*, 331-334.
1278 10.1002/jemt.10213.
1279 47. Junger, M.A., Rintelen, F., Stocker, H., Wasserman, J.D., Vegh, M., Radimerski, T., Greenberg,
1280 M.E., and Hafen, E. (2003). The Drosophila forkhead transcription factor FOXO mediates the
1281 reduction in cell number associated with reduced insulin signaling. J Biol *2*, 20. 10.1186/1475-
1282 4924-2-20.
1283 48. Martinez, S.C., Cras-Meneur, C., Bernal-Mizrachi, E., and Permutt, M.A. (2006). Glucose
1284 regulates Foxo1 through insulin receptor signaling in the pancreatic islet beta-cell. Diabetes *55*,
1285 1581-1591. 10.2337/db05-0678.
1286 49. Nagashima, T., Shigematsu, N., Maruki, R., Urano, Y., Tanaka, H., Shimaya, A., Shimokawa, T.,
1287 and Shibasaki, M. (2010). Discovery of novel forkhead box O1 inhibitors for treating type 2
1288 diabetes: improvement of fasting glycemia in diabetic db/db mice. Mol Pharmacol *78*, 961-970.
1289 10.1124/mol.110.065714.
1290 50. Pandey, A., Kumar, G.S., Kadakol, A., Malek, V., and Gaikwad, A.B. (2016). FoxO1 Inhibitors:
1291 The Future Medicine for Metabolic Disorders? Curr Diabetes Rev *12*, 223-230.
1292 10.2174/1573399811666150804104858.
1293 51. Mitsiades, C.S., Mitsiades, N.S., McMullan, C.J., Poulaki, V., Shringarpure, R., Akiyama, M.,
1294 Hideshima, T., Chauhan, D., Joseph, M., Libermann, T.A., et al. (2004). Inhibition of the insulin-
1295 like growth factor receptor-1 tyrosine kinase activity as a therapeutic strategy for multiple
1296 myeloma, other hematologic malignancies, and solid tumors. Cancer Cell *5*, 221-230.
1297 10.1016/s1535-6108(04)00050-9.
1298 52. Kawakami, Y., Rodriguez Esteban, C., Raya, M., Kawakami, H., Marti, M., Dubova, I., and
1299 Izpisua Belmonte, J.C. (2006). Wnt/beta-catenin signaling regulates vertebrate limb regeneration.
1300 Genes Dev *20*, 3232-3237. 10.1101/gad.1475106.
1301 53. Aztekin, C., Hiscock, T.W., Marioni, J.C., Gurdon, J.B., Simons, B.D., and Jullien, J. (2019).
1302 Identification of a regeneration-organizing cell in the Xenopus tail. Science *364*, 653-658.
1303 10.1126/science.aav9996.
1304 54. Srivastava, M., Mazza-Curll, K.L., van Wolfswinkel, J.C., and Reddien, P.W. (2014). Whole-body
1305 acoel regeneration is controlled by Wnt and Bmp-Admp signaling. Curr Biol *24*, 1107-1113.
1306 10.1016/j.cub.2014.03.042.
1307 55. Lander, R., and Petersen, C.P. (2016). Wnt, Ptk7, and FGFRL expression gradients control trunk
1308 positional identity in planarian regeneration. Elife *5*. 10.7554/eLife.12850.
1309 56. Petersen, C.P., and Reddien, P.W. (2009). A wound-induced Wnt expression program controls
1310 planarian regeneration polarity. Proc Natl Acad Sci U S A *106*, 17061-17066.
1311 10.1073/pnas.0906823106.
1312 57. Chen, B., Dodge, M.E., Tang, W., Lu, J., Ma, Z., Fan, C.W., Wei, S., Hao, W., Kilgore, J.,
1313 Williams, N.S., et al. (2009). Small molecule-mediated disruption of Wnt-dependent signaling in
1314 tissue regeneration and cancer. Nat Chem Biol *5*, 100-107. 10.1038/nchembio.137.
1315 58. Rodgers, J.T., King, K.Y., Brett, J.O., Cromie, M.J., Charville, G.W., Maguire, K.K., Brunson, C.,
1316 Mastey, N., Liu, L., Tsai, C.R., et al. (2014). mTORC1 controls the adaptive transition of
1317 quiescent stem cells from G0 to G(Alert). Nature *510*, 393-396. 10.1038/nature13255.
1318 59. Rodgers, J.T., Schroeder, M.D., Ma, C., and Rando, T.A. (2017). HGFA Is an Injury-Regulated
1319 Systemic Factor that Induces the Transition of Stem Cells into GAlert. Cell reports *19*, 479-486.
1320 10.1016/j.celrep.2017.03.066.
1321 60. Vander Haar, E., Lee, S.I., Bandhakavi, S., Griffin, T.J., and Kim, D.H. (2007). Insulin signalling to
1322 mTOR mediated by the Akt/PKB substrate PRAS40. Nat Cell Biol *9*, 316-323. 10.1038/ncb1547.

61. Sancak, Y., Thoreen, C.C., Peterson, T.R., Lindquist, R.A., Kang, S.A., Spooner, E., Carr, S.A., and Sabatini, D.M. (2007). PRAS40 is an insulin-regulated inhibitor of the mTORC1 protein kinase. Mol Cell *25*, 903-915. 10.1016/j.molcel.2007.03.003.
62. Koh, A., Molinaro, A., Stahlman, M., Khan, M.T., Schmidt, C., Manneras-Holm, L., Wu, H., Carreras, A., Jeong, H., Olofsson, L.E., et al. (2018). Microbially Produced Imidazole Propionate Impairs Insulin Signaling through mTORC1. Cell *175*, 947-961 e917. 10.1016/j.cell.2018.09.055.
63. Zhulyn, O., Rosenblatt, H.D., Shokat, L., Dai, S., Kuzuoglu-Ozturk, D., Zhang, Z., Ruggero, D., Shokat, K.M., and Barna, M. (2023). Evolutionarily divergent mTOR remodels translatome for tissue regeneration. Nature *620*, 163-171. 10.1038/s41586-023-06365-1.
64. Takeuchi, K., Shibamoto, S., Nagamine, K., Shigemori, I., Omura, S., Kitamura, N., and Ito, F. (2001). Signaling pathways leading to transcription and translation cooperatively regulate the transient increase in expression of c-Fos protein. J Biol Chem *276*, 26077-26083. 10.1074/jbc.M102704200.
65. Rodgers, J.T., King, K.Y., Brett, J.O., Cromie, M.J., Charville, G.W., Maguire, K.K., Brunson, C., Mastey, N., Liu, L., Tsai, C.R., et al. (2014). mTORC1 controls the adaptive transition of quiescent stem cells from G(0) to G(Alert). Nature *510*, 393-396. 10.1038/nature13255.
66. Brown, E.J., Albers, M.W., Shin, T.B., Ichikawa, K., Keith, C.T., Lane, W.S., and Schreiber, S.L. (1994). A mammalian protein targeted by G1-arresting rapamycin-receptor complex. Nature *369*, 756-758. 10.1038/369756a0.
67. Saxton, R.A., and Sabatini, D.M. (2017). mTOR Signaling in Growth, Metabolism, and Disease. Cell *168*, 960-976. 10.1016/j.cell.2017.02.004.
68. Renthal, W., Tochitsky, I., Yang, L., Cheng, Y.C., Li, E., Kawaguchi, R., Geschwind, D.H., and Woolf, C.J. (2020). Transcriptional Reprogramming of Distinct Peripheral Sensory Neuron Subtypes after Axonal Injury. Neuron *108*, 128-144 e129. 10.1016/j.neuron.2020.07.026.
69. Todd, J.T. (1823). On the process of reproduction of the members of the aquatic salamander. . The Quarterly Journal of Science, Literature, and the Arts. *16*, 84-96.
70. Singer, M. (1946). The nervous system and regeneration of the forelimb of adult Triturus; the influence of number of nerve fibers, including a quantitative study of limb innervation. J Exp Zool *101*, 299-337.
71. Singer, M. (1952). The influence of the nerve in regeneration of the amphibian extremity. Q Rev Biol *27*, 169-200.
72. Brockes, J.P. (1987). The nerve dependence of amphibian limb regeneration. The Journal of experimental biology *132*, 79-91.
73. Farkas, J.E., and Monaghan, J.R. (2017). A brief history of the study of nerve dependent regeneration. Neurogenesis (Austin) *4*, e1302216. 10.1080/23262133.2017.1302216.
74. Wells, K.M., Kelley, K., Baumel, M., Vieira, W.A., and McCusker, C.D. (2021). Neural control of growth and size in the axolotl limb regenerate. Elife *10*. 10.7554/eLife.68584.
75. Johnson, C.K., and Voss, S.R. (2013). Salamander paedomorphosis: linking thyroid hormone to life history and life cycle evolution. Curr Top Dev Biol *103*, 229-258. 10.1016/B978-0-12-385979-2.00008-3.
76. Collins, J.P., Cheek, J.E. (1983). Effect of Food and Density on Development of Typical and Cannibalistic Salamander Larvae in Ambystoma tigrinum nebulosum. Integr Comp Biol *23*, 77-84.
77. Villiard, E., Brinkmann, H., Moiseeva, O., Mallette, F.A., Ferbeyre, G., and Roy, S. (2007). Urodele p53 tolerates amino acid changes found in p53 variants linked to human cancer. BMC evolutionary biology *7*, 180. 10.1186/1471-2148-7-180.
78. Wong, A.Y., and Whited, J.L. (2020). Parallels between wound healing, epimorphic regeneration and solid tumors. Development *147*. 10.1242/dev.181636.
79. Yun, M.H. (2021). Salamander Insights Into Ageing and Rejuvenation. Front Cell Dev Biol *9*, 689062. 10.3389/fcell.2021.689062.
80. Breedis, C. (1952). Induction of accessory limbs and of sarcoma in the Newt (Triturus viridescens) with carcinogenic substances. Cancer research *12*, 861-866.
81. Ingram, A.J. (1971). The reactions to carcinogens in the axolotl (Ambystoma mexicanum) in relation to the "regeneration field control" hypothesis. J Embryol Exp Morphol *26*, 425-441.
82. Tsonis, P.A. (1983). Effects of carcinogens on regenerating and non-regenerating limbs in amphibia (review). Anticancer Res *3*, 195-202.

83. Tsonis, P.A., and Eguchi, G. (1981). Carcinogens on regeneration. Effects of N-methyl-N'-nitro-N-nitrosoguanidine and 4-nitroquinoline-1-oxide on limb regeneration in adult newts. Differentiation *20*, 52-60.
84. Seilern-Aspang, F., and Kratochwil, K. (1962). Induction and differentiation of an epithelial tumour in the newt (Triturus cristatus). J Embryol Exp Morphol *10*, 337-356.
85. Waddington, C.H. (1935). Cancer and the theory of organisers. Nature *135*, 606-608.
86. Crawford, L.V., Pim, D.C., Gurney, E.G., Goodfellow, P., and Taylor-Papadimitriou, J. (1981). Detection of a common feature in several human tumor cell lines--a 53,000-dalton protein. Proc Natl Acad Sci U S A *78*, 41-45. 10.1073/pnas.78.1.41.
87. Haber, D.A., Buckler, A.J., Glaser, T., Call, K.M., Pelletier, J., Sohn, R.L., Douglass, E.C., and Housman, D.E. (1990). An internal deletion within an 11p13 zinc finger gene contributes to the development of Wilms' tumor. Cell *61*, 1257-1269. 10.1016/0092-8674(90)90690-g.
88. Hara, M.R., Kovacs, J.J., Whalen, E.J., Rajagopal, S., Strachan, R.T., Grant, W., Towers, A.J., Williams, B., Lam, C.M., Xiao, K., et al. (2011). A stress response pathway regulates DNA damage through beta2-adrenoreceptors and beta-arrestin-1. Nature *477*, 349-353. 10.1038/nature10368.
89. Hara, M.R., Sachs, B.D., Caron, M.G., and Lefkowitz, R.J. (2013). Pharmacological blockade of a beta(2)AR-beta-arrestin-1 signaling cascade prevents the accumulation of DNA damage in a behavioral stress model. Cell Cycle *12*, 219-224. 10.4161/cc.23368.
90. Bryant, D.M., Sousounis, K., Payzin-Dogru, D., Bryant, S., Sandoval, A.G.W., Martinez Fernandez, J., Mariano, R., Oshiro, R., Wong, A.Y., Leigh, N.D., et al. (2017). Identification of regenerative roadblocks via repeat deployment of limb regeneration in axolotls. NPJ Regen Med *2*, 30. 10.1038/s41536-017-0034-z.
91. Dearlove, G.E., and Dresden, M.H. (1976). Regenerative abnormalities in Notophthalmus viridescens induced by repeated amputations. The Journal of experimental zoology *196*, 251-262. 10.1002/jez.1401960212.
92. Stone, R.C., Pastar, I., Ojeh, N., Chen, V., Liu, S., Garzon, K.I., and Tomic-Canic, M. (2016). Epithelial-mesenchymal transition in tissue repair and fibrosis. Cell and Tissue Research *365*, 495-506. 10.1007/s00441-016-2464-0.
93. Keel, M., and Trentz, O. (2005). Pathophysiology of polytrauma. Injury *36*, 691-709. 10.1016/j.injury.2004.12.037.
94. Khattak, S., Schuez, M., Richter, T., Knapp, D., Haigo, S.L., Sandoval-Guzman, T., Hradlikova, K., Duemmler, A., Kerney, R., and Tanaka, E.M. (2013). Germline transgenic methods for tracking cells and testing gene function during regeneration in the axolotl. Stem Cell Reports *1*, 90-103. 10.1016/j.stemcr.2013.03.002.
95. Schotté, O.E., and Butler, E.G. (1941). Morphological effects of denervation and amputation of limbs in urodele larvae. Journal of Experimental Zoology *87*, 279-322. https://doi.org/10.1002/jez.1400870207.
96. Kropf, N., Krishnan, K., Chao, M., Schweitzer, M., Rosenberg, Z., and Russell, S.M. (2010). Sciatic nerve injury model in the axolotl: functional, electrophysiological, and radiographic outcomes. J Neurosurg *112*, 880-889. 10.3171/2008.10.Jns08222.
97. Lovely, A.M., Duerr, T.J., Stein, D.F., Mun, E.T., and Monaghan, J.R. (2022). Hybridization Chain Reaction Fluorescence In Situ Hybridization (HCR-FISH) in Ambystoma mexicanum Tissue. In Salamanders: Methods and Protocols, (Springer), pp. 109-122.
98. Debuque, R.J., and Godwin, J.W. (2015). Methods for axolotl blood collection, intravenous injection, and efficient leukocyte isolation from peripheral blood and the regenerating limb. Methods Mol Biol *1290*, 205-226. 10.1007/978-1-4939-2495-0_17.
99. McQuin, C., Goodman, A., Chernyshev, V., Kamentsky, L., Cimini, B.A., Karhohs, K.W., Doan, M., Ding, L., Rafelski, S.M., Thirstrup, D., et al. (2018). CellProfiler 3.0: Next-generation image processing for biology. PLOS Biology *16*, e2005970. 10.1371/journal.pbio.2005970.
100. Schindelin, J., Arganda-Carreras, I., Frise, E., Kaynig, V., Longair, M., Pietzsch, T., Preibisch, S., Rueden, C., Saalfeld, S., Schmid, B., et al. (2012). Fiji: an open-source platform for biological-image analysis. Nature Methods *9*, 676-682. 10.1038/nmeth.2019.
101. Bolger, A.M., Lohse, M., and Usadel, B. (2014). Trimmomatic: a flexible trimmer for Illumina sequence data. Bioinformatics *30*, 2114-2120. 10.1093/bioinformatics/btu170.

102. Bray, N.L., Pimentel, H., Melsted, P., and Pachter, L. (2016). Near-optimal probabilistic RNA-seq quantification. Nat Biotechnol *34*, 525-527. 10.1038/nbt.3519.
103. Soneson, C., Love, M.I., and Robinson, M.D. (2015). Differential analyses for RNA-seq: transcript-level estimates improve gene-level inferences. F1000Res *4*, 1521. 10.12688/f1000research.7563.2.
104. Love, M.I., Huber, W., and Anders, S. (2014). Moderated estimation of fold change and dispersion for RNA-seq data with DESeq2. Genome biology *15*, 550. 10.1186/s13059-014-0550-8.
105. Kolde, R. (2019). pheatmap: Pretty Heatmaps. R package version 1.0. 12. R Packag. version 1.0 *8*.
106. Ulgen, E., Ozisik, O., and Sezerman, O.U. (2019). pathfindR: An R Package for Comprehensive Identification of Enriched Pathways in Omics Data Through Active Subnetworks. Front Genet *10*, 858. 10.3389/fgene.2019.00858.
107. Grabherr, M.G., Haas, B.J., Yassour, M., Levin, J.Z., Thompson, D.A., Amit, I., Adiconis, X., Fan, L., Raychowdhury, R., Zeng, Q., et al. (2011). Full-length transcriptome assembly from RNA-Seq data without a reference genome. Nat Biotechnol *29*, 644-652. 10.1038/nbt.1883.
108. Schloissnig, S., Kawaguchi, A., Nowoshilow, S., Falcon, F., Otsuki, L., Tardivo, P., Timoshevskaya, N., Keinath, M.C., Smith, J.J., Voss, S.R., and Tanaka, E.M. (2021). The giant axolotl genome uncovers the evolution, scaling, and transcriptional control of complex gene loci. Proc Natl Acad Sci U S A *118*. 10.1073/pnas.2017176118.
109. Li, H. (2018). Minimap2: pairwise alignment for nucleotide sequences. Bioinformatics *34*, 3094-3100. 10.1093/bioinformatics/bty191.
110. Li, H., Handsaker, B., Wysoker, A., Fennell, T., Ruan, J., Homer, N., Marth, G., Abecasis, G., and Durbin, R. (2009). The Sequence Alignment/Map format and SAMtools. Bioinformatics *25*, 2078-2079. 10.1093/bioinformatics/btp352.
111. Neph, S., Kuehn, M.S., Reynolds, A.P., Haugen, E., Thurman, R.E., Johnson, A.K., Rynes, E., Maurano, M.T., Vierstra, J., Thomas, S., et al. (2012). BEDOPS: high-performance genomic feature operations. Bioinformatics *28*, 1919-1920. 10.1093/bioinformatics/bts277.
112. Arnason, U., Gullberg, A., Janke, A., Joss, J., and Elmerot, C. (2004). Mitogenomic analyses of deep gnathostome divergences: a fish is a fish. Gene *333*, 61-70. 10.1016/j.gene.2004.02.014.
113. Quinlan, A.R., and Hall, I.M. (2010). BEDTools: a flexible suite of utilities for comparing genomic features. Bioinformatics *26*, 841-842. 10.1093/bioinformatics/btq033.
114. Gao, F., da Veiga Beltrame, E., Gehring, J.A., Edljarn Hjoerleifsson, K.E., Lu, L., Melsted, P., Ntranos, V., Pachter, L., and Svensson, V. (2019). The BUS Format for Single-Cell RNA-Seq Processing and Analysis. J Biomol Tech *30*, S62-S62.
115. Melsted, P., Booeshaghi, A.S., Liu, L., Gao, F., Lu, L., Min, K.H.J., da Veiga Beltrame, E., Hjörleifsson, K.E., Gehring, J., and Pachter, L. (2021). Modular, efficient and constant-memory single-cell RNA-seq preprocessing. Nat Biotechnol *39*, 813-818. 10.1038/s41587-021-00870-2.
116. Moses L, P.L. (2022). BUSpaRse: kallisto | bustools R utilities.
117. Hao, Y., Hao, S., Andersen-Nissen, E., Mauck, W.M., 3rd, Zheng, S., Butler, A., Lee, M.J., Wilk, A.J., Darby, C., Zager, M., et al. (2021). Integrated analysis of multimodal single-cell data. Cell *184*, 3573-3587.e3529. 10.1016/j.cell.2021.04.048.
118. Wickham, H. (2009). Elegant graphics for data analysis (ggplot2). Applied Spatial Data Analysis R.
119. Jin, S., Guerrero-Juarez, C.F., Zhang, L., Chang, I., Ramos, R., Kuan, C.-H., Myung, P., Plikus, M.V., and Nie, Q. (2021). Inference and analysis of cell-cell communication using CellChat. Nature communications *12*, 1088. 10.1038/s41467-021-21246-9.
120. La Manno, G., Soldatov, R., Zeisel, A., Braun, E., Hochgerner, H., Petukhov, V., Lidschreiber, K., Kastriti, M.E., Lönnerberg, P., Furlan, A., et al. (2018). RNA velocity of single cells. Nature *560*, 494-498. 10.1038/s41586-018-0414-6.
121. Bergen, V., Lange, M., Peidli, S., Wolf, F.A., and Theis, F.J. (2020). Generalizing RNA velocity to transient cell states through dynamical modeling. Nature Biotechnology *38*, 1408-1414. 10.1038/s41587-020-0591-3.
122. Langmead, B., and Salzberg, S.L. (2012). Fast gapped-read alignment with Bowtie 2. Nat Methods *9*, 357-359. 10.1038/nmeth.1923.

123. Li, H., Handsaker, B., Wysoker, A., Fennell, T., Ruan, J., Homer, N., Marth, G., Abecasis, G., Durbin, R., and Subgroup, G.P.D.P. (2009). The Sequence Alignment/Map format and SAMtools. Bioinformatics *25*, 2078-2079. 10.1093/bioinformatics/btp352.
124. Picard Toolkit. (2019). https://broadinstitute.github.io/picard/.
125. Ramírez, F., Ryan, D.P., Grüning, B., Bhardwaj, V., Kilpert, F., Richter, A.S., Heyne, S., Dündar, F., and Manke, T. (2016). deepTools2: a next generation web server for deep-sequencing data analysis. Nucleic Acids Res *44*, W160-165. 10.1093/nar/gkw257.
126. Zhang, Y., Liu, T., Meyer, C.A., Eeckhoute, J., Johnson, D.S., Bernstein, B.E., Nusbaum, C., Myers, R.M., Brown, M., Li, W., and Liu, X.S. (2008). Model-based analysis of ChIP-Seq (MACS). Genome Biol *9*, R137. 10.1186/gb-2008-9-9-r137.
127. Wang, Q., Li, M., Wu, T., Zhan, L., Li, L., Chen, M., Xie, W., Xie, Z., Hu, E., Xu, S., and Yu, G. (2022). Exploring Epigenomic Datasets by ChIPseeker. Curr Protoc *2*, e585. 10.1002/cpz1.585.
128. Liao, Y., Smyth, G.K., and Shi, W. (2014). featureCounts: an efficient general purpose program for assigning sequence reads to genomic features. Bioinformatics *30*, 923-930. 10.1093/bioinformatics/btt656.
129. Kolde, R. (2019). pheatmap: pretty heatmaps. R package version 1.0. 12. 2019.
130. Marini, F., and Binder, H. (2019). pcaExplorer: an R/Bioconductor package for interacting with RNA-seq principal components. BMC Bioinformatics *20*, 331. 10.1186/s12859-019-2879-1.
131. Heinz, S., Benner, C., Spann, N., Bertolino, E., Lin, Y.C., Laslo, P., Cheng, J.X., Murre, C., Singh, H., and Glass, C.K. (2010). Simple combinations of lineage-determining transcription factors prime cis-regulatory elements required for macrophage and B cell identities. Mol Cell *38*, 576-589. 10.1016/j.molcel.2010.05.004.
132. Hao, Y., Stuart, T., Kowalski, M.H., Choudhary, S., Hoffman, P., Hartman, A., Srivastava, A., Molla, G., Madad, S., Fernandez-Granda, C., and Satija, R. (2024). Dictionary learning for integrative, multimodal and scalable single-cell analysis. Nat Biotechnol *42*, 293-304. 10.1038/s41587-023-01767-y.
133. Mi, H., Muruganujan, A., Huang, X., Ebert, D., Mills, C., Guo, X., and Thomas, P.D. (2019). Protocol Update for large-scale genome and gene function analysis with the PANTHER classification system (v.14.0). Nat Protoc *14*, 703-721. 10.1038/s41596-019-0128-8.
134. Wickham, H. (2016). ggplot2: Elegant Graphics for Data Analysis (Springer-Verlag New York).
135. Altschul, S.F., Gish, W., Miller, W., Myers, E.W., and Lipman, D.J. (1990). Basic local alignment search tool. J Mol Biol *215*, 403-410. 10.1016/s0022-2836(05)80360-2.
136. Tarashansky, A.J., Musser, J.M., Khariton, M., Li, P., Arendt, D., Quake, S.R., and Wang, B. (2021). Mapping single-cell atlases throughout Metazoa unravels cell type evolution. Elife *10*. 10.7554/eLife.66747.
137. Galili, T., O'Callaghan, A., Sidi, J., and Sievert, C. (2018). heatmaply: an R package for creating interactive cluster heatmaps for online publishing. Bioinformatics *34*, 1600-1602. 10.1093/bioinformatics/btx657.
138. Carpenter, A.E., Jones, T.R., Lamprecht, M.R., Clarke, C., Kang, I.H., Friman, O., Guertin, D.A., Chang, J.H., Lindquist, R.A., Moffat, J., et al. (2006). CellProfiler: image analysis software for identifying and quantifying cell phenotypes. Genome biology *7*, R100. 10.1186/gb-2006-7-10-r100.
139. Bray, N.L., Pimentel, H., Melsted, P., and Pachter, L. (2016). Near-optimal probabilistic RNA-seq quantification. Nature Biotechnology *34*, 525-527. 10.1038/nbt.3519.
140. Kent, W.J., Zweig, A.S., Barber, G., Hinrichs, A.S., and Karolchik, D. (2010). BigWig and BigBed: enabling browsing of large distributed datasets. Bioinformatics *26*, 2204-2207. 10.1093/bioinformatics/btq351.
141. Li, Q., Brown, J.B., Huang, H., and Bickel, P.J. (2011). Measuring reproducibility of high-throughput experiments. The Annals of Applied Statistics *5*, 1752-1779, 1728.
142. Yu, G., Wang, L.-G., and He, Q.-Y. (2015). ChIPseeker: an R/Bioconductor package for ChIP peak annotation, comparison and visualization. Bioinformatics *31*, 2382-2383. 10.1093/bioinformatics/btv145.

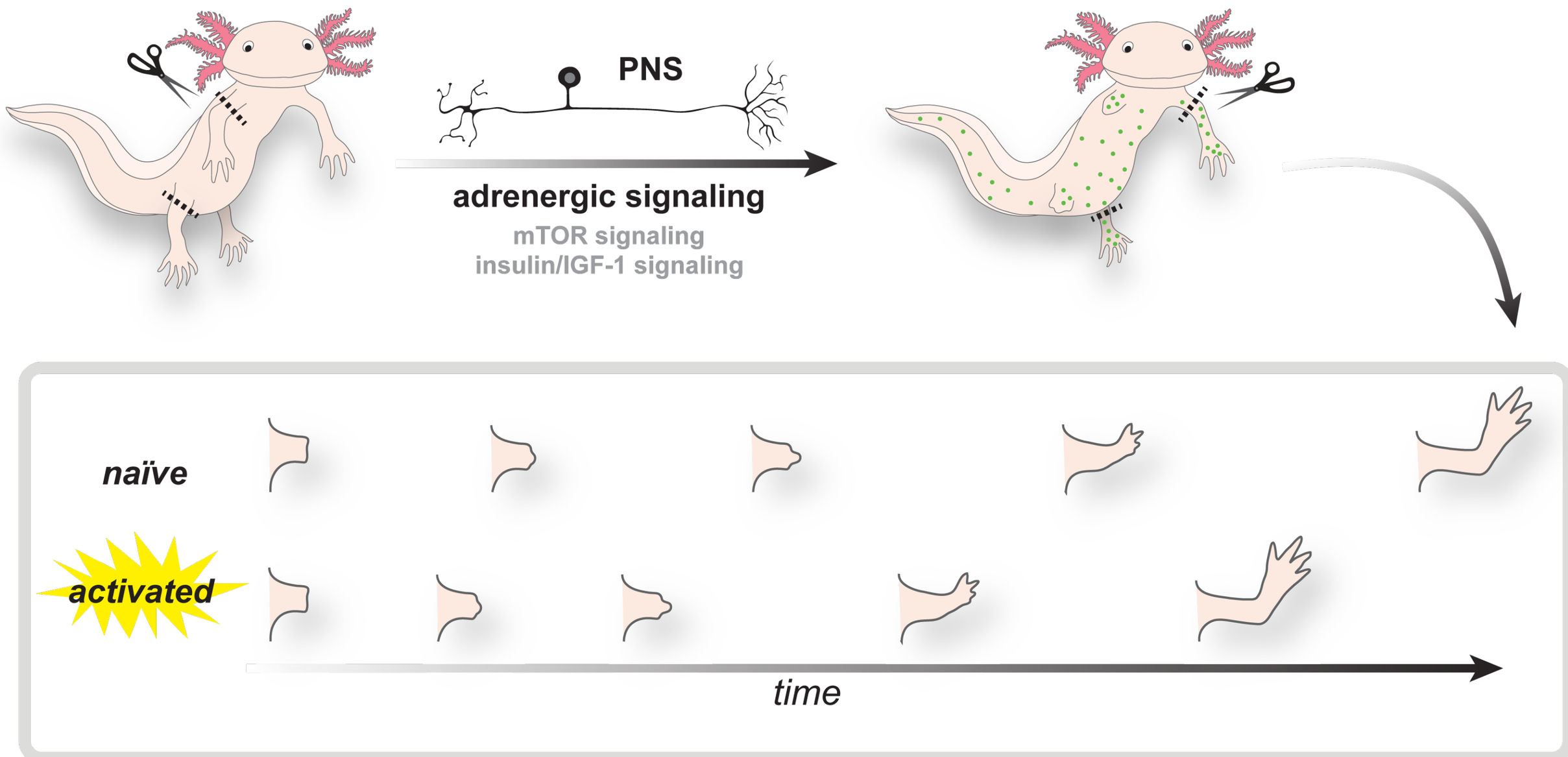

HIGHLIGHTS

- Systemic stem cell activation following amputation promotes faster regeneration
- Nerves and adrenergic signaling are required for systemic cell cycle re-entry
- Systemically-activated cell types are shared with proliferating cell types in homeostasis
- Systemic activation is accompanied by global epigenetic changes in distant tissues

IN BRIEF

Payzin-Dogru *et al.* demonstrate amputation-induced systemic cell activation response in axolotl primes distant appendages for faster regeneration and identify the peripheral nervous system as an essential input regulating this response. Transcriptomics and functional experimentation reveal adrenergic signaling as a key molecular pathway triggering systemic cell activation.

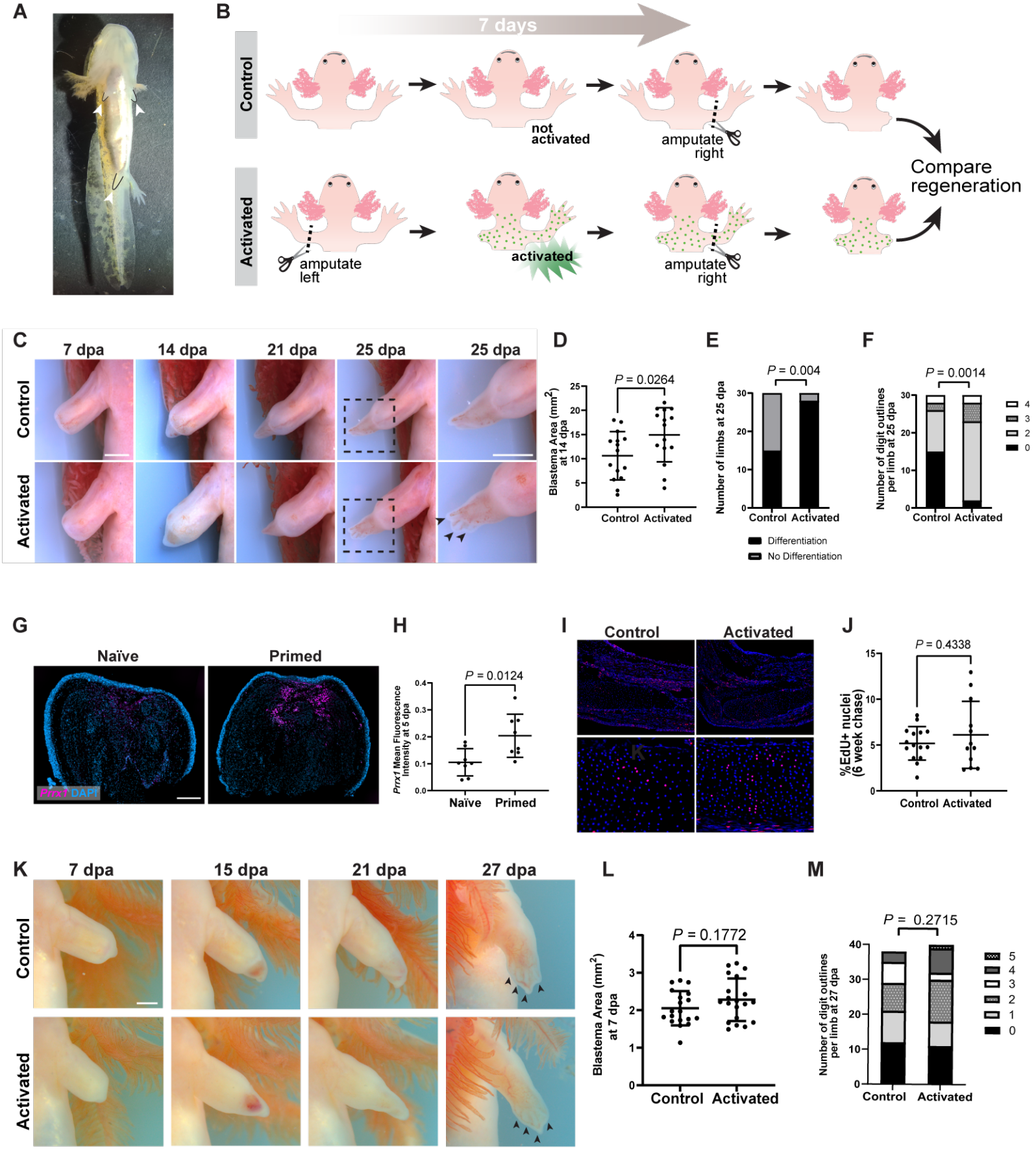
A
B
7 days
Control
Activated
not activated
amputate right
amputate left
activated
amputate right
Compare regeneration
C
7 dpa
14 dpa
21 dpa
25 dpa
25 dpa
Control
Activated
D
P = 0.0264
Blastema Area (mm2) at 14 dpa
Control
Activated
E
P = 0.004
Number of limbs at 25 dpa
Control
Activated
Differentiation
No Differentiation
F
P = 0.0014
Number of digit outlines per limb at 25 dpa
Control
Activated
4
3
2
0
G
Naïve
Primed
Prrx1 DAPI
H
P = 0.0124
Prrx1 Mean Fluorescence Intensity at 5 dpa
Naïve
Primed
I
Control
Activated
J
P = 0.4338
%EdU+ nuclei (6 week chase)
Control
Activated
K
7 dpa
15 dpa
21 dpa
27 dpa
Control
Activated
L
P = 0.1772
Blastema Area (mm2) at 7 dpa
Control
Activated
M
P = 0.2715
Number of digit outlines per limb at 27 dpa
Control
Activated
5
4
3
2
1
0

Figure 1

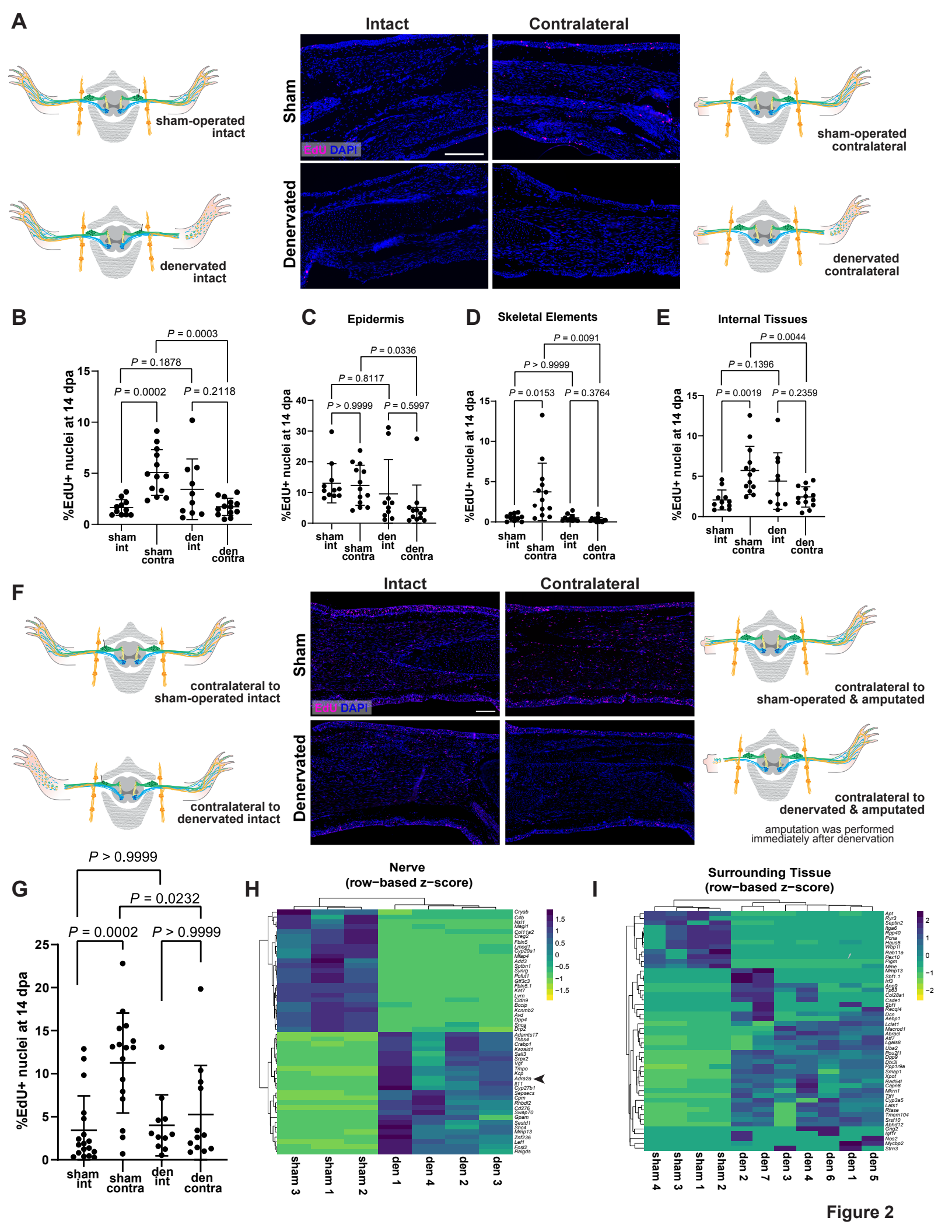
A
Intact
Contralateral
Sham
Denervated
EdU DAPI
sham-operated intact
denervated intact
sham-operated contralateral
denervated contralateral
B
%EdU+ nuclei at 14 dpa
P = 0.0003
P = 0.1878
P = 0.0002
P = 0.2118
sham int
sham contra
den int
den contra
C
Epidermis
P = 0.0336
P = 0.8117
P > 0.9999
P = 0.5997
D
Skeletal Elements
P = 0.0091
P > 0.9999
P = 0.0153
P = 0.3764
E
Internal Tissues
P = 0.0044
P = 0.1396
P = 0.0019
P = 0.2359
F
contralateral to sham-operated intact
contralateral to denervated intact
contralateral to sham-operated & amputated
contralateral to denervated & amputated
amputation was performed immediately after denervation
G
P > 0.9999
P = 0.0232
P = 0.0002
P > 0.9999
H
Nerve (row−based z−score)
sham 3
sham 1
sham 2
den 1
den 4
den 2
den 3
I
Surrounding Tissue (row−based z−score)
sham 4
sham 3
sham 1
sham 2
den 2
den 7
den 3
den 4
den 6
den 1
den 5

Figure 2

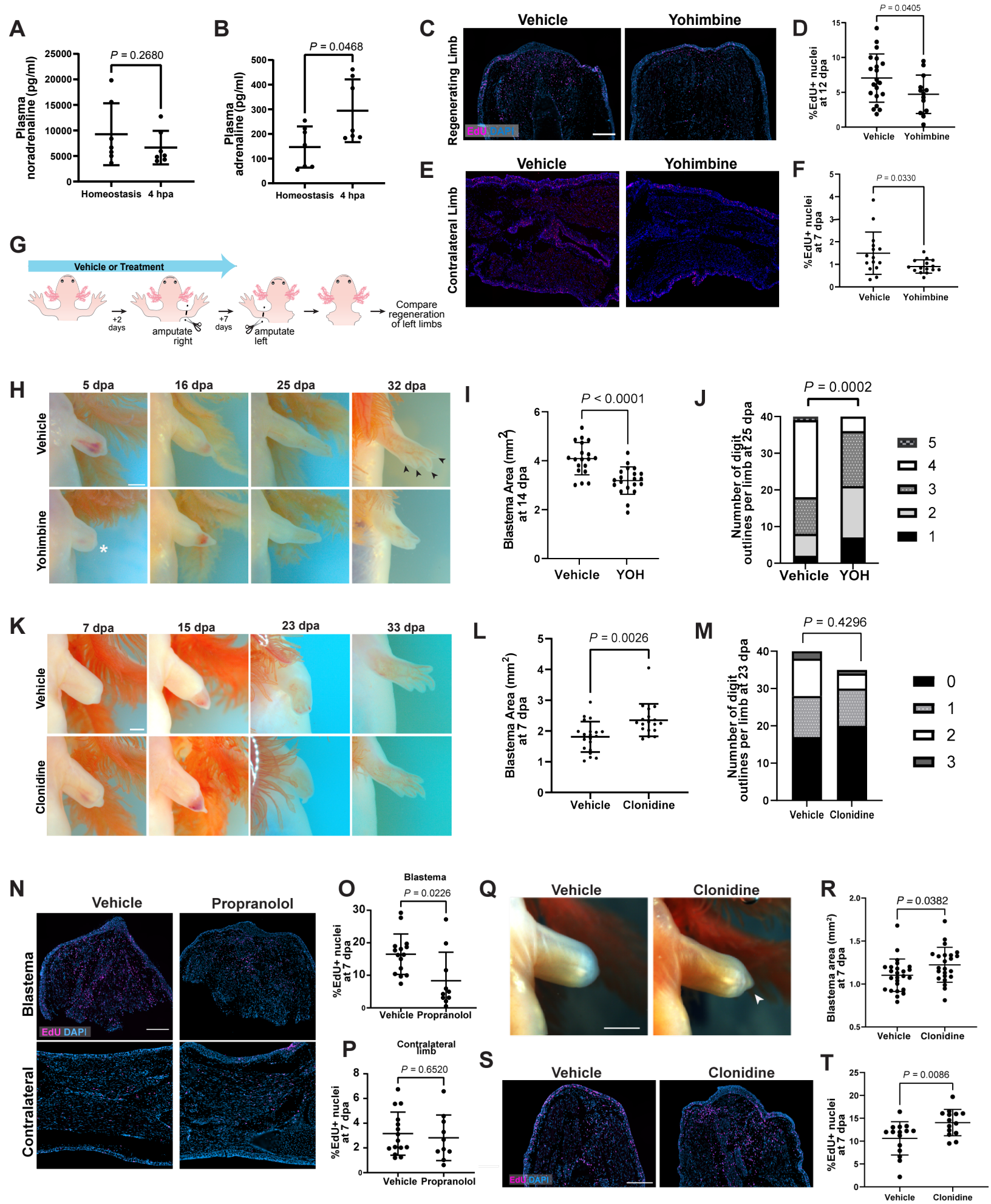
A
Plasma noradrenaline (pg/ml)
P = 0.2680
Homeostasis
4 hpa
B
Plasma adrenaline (pg/ml)
P = 0.0468
Homeostasis
4 hpa
C
Vehicle
Yohimbine
Regenerating Limb
EdU DAPI
D
%EdU+ nuclei at 12 dpa
P = 0.0405
Vehicle
Yohimbine
E
Vehicle
Yohimbine
Contralateral Limb
F
%EdU+ nuclei at 7 dpa
P = 0.0330
Vehicle
Yohimbine
G
Vehicle or Treatment
+2 days
amputate right
+7 days
amputate left
Compare regeneration of left limbs
H
5 dpa
16 dpa
25 dpa
32 dpa
Vehicle
Yohimbine
I
Blastema Area (mm2) at 14 dpa
P < 0.0001
Vehicle
YOH
J
Numnber of digit outlines per limb at 25 dpa
P = 0.0002
Vehicle
YOH
5
4
3
2
1
K
7 dpa
15 dpa
23 dpa
33 dpa
Vehicle
Clonidine
L
Blastema Area (mm2) at 7 dpa
P = 0.0026
Vehicle
Clonidine
M
Numnber of digit outlines per limb at 23 dpa
P = 0.4296
Vehicle
Clonidine
0
1
2
3
N
Vehicle
Propranolol
Blastema
Contralateral
EdU DAPI
O
Blastema
%EdU+ nuclei at 7 dpa
P = 0.0226
Vehicle
Propranolol
P
Contralateral limb
%EdU+ nuclei at 7 dpa
P = 0.6520
Vehicle
Propranolol
Q
Vehicle
Clonidine
R
Blastema area (mm2) at 7 dpa
P = 0.0382
Vehicle
Clonidine
S
Vehicle
Clonidine
EdU DAPI
T
%EdU+ nuclei at 7 dpa
P = 0.0086
Vehicle
Clonidine

Figure 3

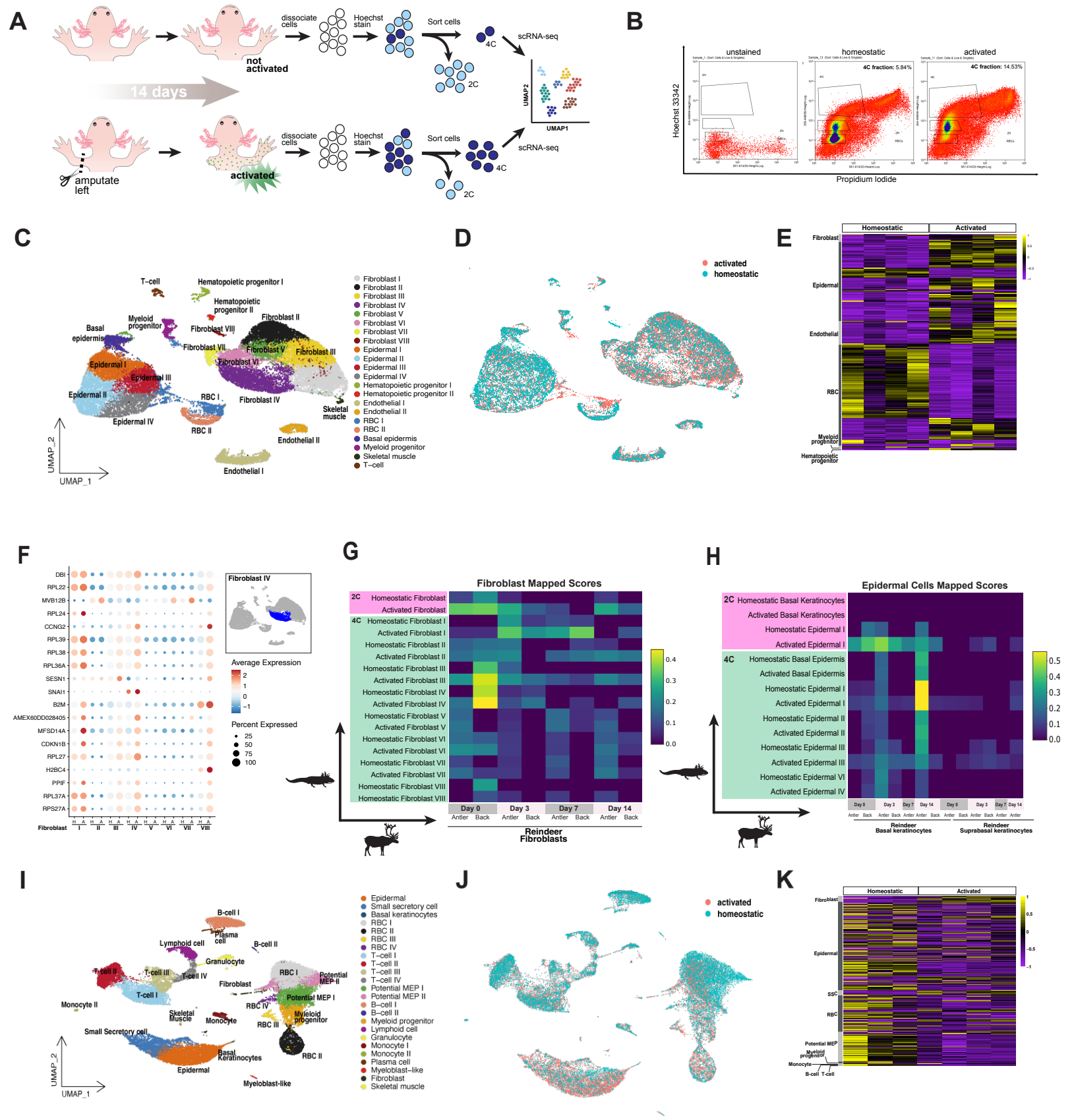
A
not activated
14 days
amputate left
activated
dissociate cells
Hoechst stain
Sort cells
4C
2C
scRNA-seq
UMAP2
UMAP1
B
unstained
homeostatic
activated
4C fraction: 5.84%
4C fraction: 14.53%
Hoechst 33342
Propidium Iodide
C
T-cell
Hematopoietic progenitor I
Hematopoietic progenitor II
Myeloid progenitor
Basal epidermis
Fibroblast VIII
Fibroblast VII
Fibroblast II
Fibroblast V
Fibroblast III
Fibroblast VI
Epidermal I
Epidermal III
Epidermal II
RBC I
Fibroblast IV
Skeletal muscle
Epidermal IV
RBC II
Endothelial II
Endothelial I
UMAP_2
UMAP_1
Fibroblast I
Fibroblast II
Fibroblast III
Fibroblast IV
Fibroblast V
Fibroblast VI
Fibroblast VII
Fibroblast VIII
Epidermal I
Epidermal II
Epidermal III
Epidermal IV
Hematopoietic progenitor I
Hematopoietic progenitor II
Endothelial I
Endothelial II
RBC I
RBC II
Basal epidermis
Myeloid progenitor
Skeletal muscle
T-cell
D
activated
homeostatic
E
Homeostatic
Activated
Fibroblast
Epidermal
Endothelial
RBC
Myeloid progenitor
Hematopoietic progenitor
F
DBI
RPL22
MVB12B
RPL24
CCNG2
RPL39
RPL38
RPL36A
SESN1
SNAI1
B2M
AMEX60DD028405
MFSD14A
CDKN1B
RPL27
H2BC4
PPIF
RPL37A
RPS27A
Fibroblast
Fibroblast IV
Average Expression
Percent Expressed
G
Fibroblast Mapped Scores
2C Homeostatic Fibroblast
Activated Fibroblast
4C Homeostatic Fibroblast I
Activated Fibroblast I
Homeostatic Fibroblast II
Activated Fibroblast II
Homeostatic Fibroblast III
Activated Fibroblast III
Homeostatic Fibroblast IV
Activated Fibroblast IV
Homeostatic Fibroblast V
Activated Fibroblast V
Homeostatic Fibroblast VI
Activated Fibroblast VI
Homeostatic Fibroblast VII
Activated Fibroblast VII
Homeostatic Fibroblast VIII
Day 0
Day 3
Day 7
Day 14
Antler
Back
Reindeer Fibroblasts
H
Epidermal Cells Mapped Scores
2C Homeostatic Basal Keratinocytes
Activated Basal Keratinocytes
Homeostatic Epidermal I
Activated Epidermal I
4C Homeostatic Basal Epidermis
Activated Basal Epidermis
Homeostatic Epidermal I
Activated Epidermal I
Homeostatic Epidermal II
Activated Epidermal II
Homeostatic Epidermal III
Activated Epidermal III
Homeostatic Epidermal VI
Activated Epidermal IV
Reindeer Basal keratinocytes
Reindeer Suprabasal keratinocytes
I
B-cell I
Plasma cell
Lymphoid cell
B-cell II
Granulocyte
T-cell II
T-cell III
T-cell IV
T-cell I
Fibroblast
RBC I
Potential MEP II
Potential MEP I
Monocyte II
Skeletal Muscle
Monocyte
RBC IV
RBC III
Myeloid progenitor
Small Secretory cell
Basal Keratinocytes
RBC II
Epidermal
Myeloblast-like
UMAP_2
UMAP_1
Epidermal
Small secretory cell
Basal keratinocytes
RBC I
RBC II
RBC III
RBC IV
T-cell I
T-cell II
T-cell III
T-cell IV
Potential MEP I
Potential MEP II
B-cell I
B-cell II
Myeloid progenitor
Lymphoid cell
Granulocyte
Monocyte I
Monocyte II
Plasma cell
Myeloblast-like
Fibroblast
Skeletal muscle
J
activated
homeostatic
K
Homeostatic
Activated
Fibroblast
Epidermal
SSC
RBC
Potential MEP
Myeloid progenitor
Monocyte
B-cell
T-cell

Figure 4

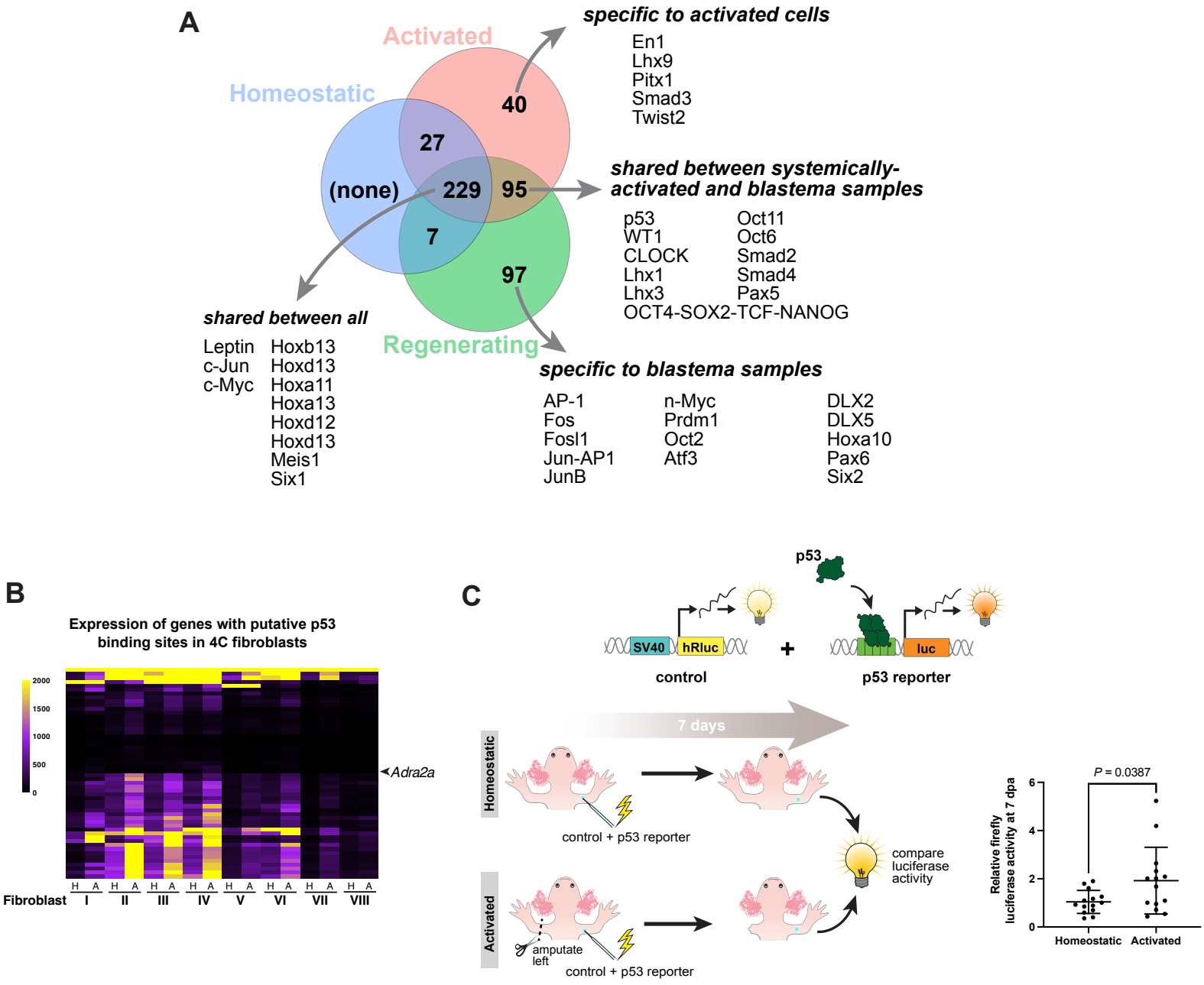
A
Activated
Homeostatic
Regenerating
40
27
(none)
229
95
7
97
specific to activated cells
En1
Lhx9
Pitx1
Smad3
Twist2
shared between systemically-activated and blastema samples
p53
WT1
CLOCK
Lhx1
Lhx3
OCT4-SOX2-TCF-NANOG
Oct11
Oct6
Smad2
Smad4
Pax5
shared between all
Leptin
c-Jun
c-Myc
Hoxb13
Hoxd13
Hoxa11
Hoxa13
Hoxd12
Hoxd13
Meis1
Six1
specific to blastema samples
AP-1
Fos
Fosl1
Jun-AP1
JunB
n-Myc
Prdm1
Oct2
Atf3
DLX2
DLX5
Hoxa10
Pax6
Six2
B
Expression of genes with putative p53 binding sites in 4C fibroblasts
2000
1500
1000
500
0
Adra2a
H A H A H A H A H A H A H A H A
Fibroblast I II III IV V VI VII VIII
C
p53
SV40
hRluc
control
luc
p53 reporter
7 days
Homeostatic
control + p53 reporter
Activated
amputate left
control + p53 reporter
compare luciferase activity
Relative firefly luciferase activity at 7 dpa
P = 0.0387
6
4
2
0
Homeostatic
Activated

Figure 5

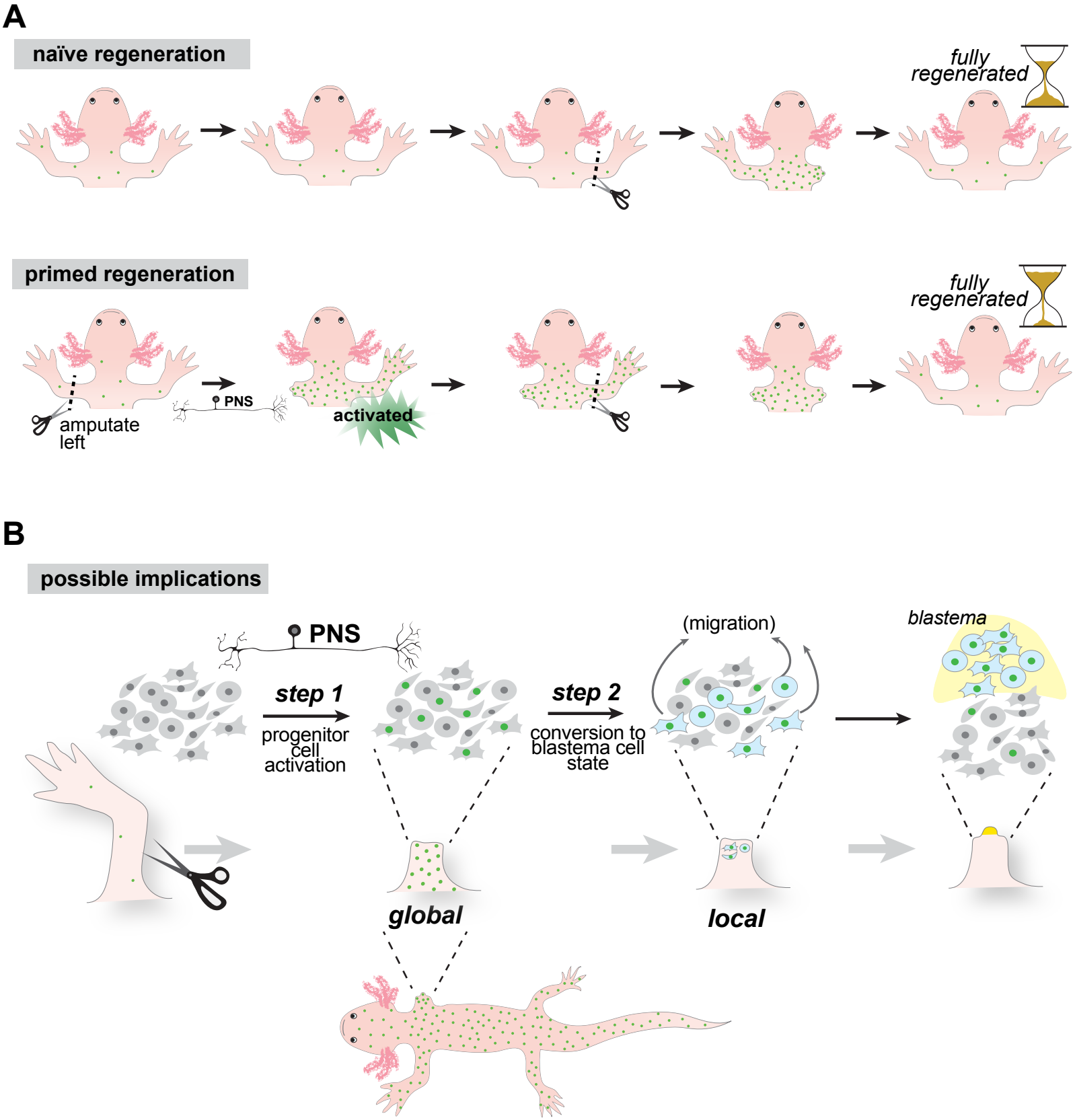
A
naïve regeneration
fully regenerated
primed regeneration
fully regenerated
amputate left
PNS
activated
B
possible implications
PNS
step 1
progenitor cell activation
step 2
conversion to blastema cell state
(migration)
blastema
global
local

Figure 6

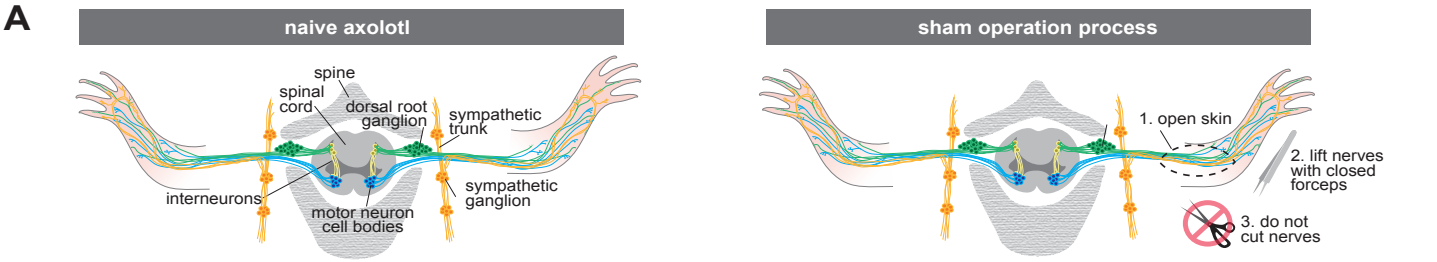

Note: aspects not drawn to scale; midline shown as transverse except with respect to sympathetic ganglia

Note: denervations are performed identically to shams, except nerves are cut; they subseqently degenerate distally and are shown as dashed lines in main figure panels

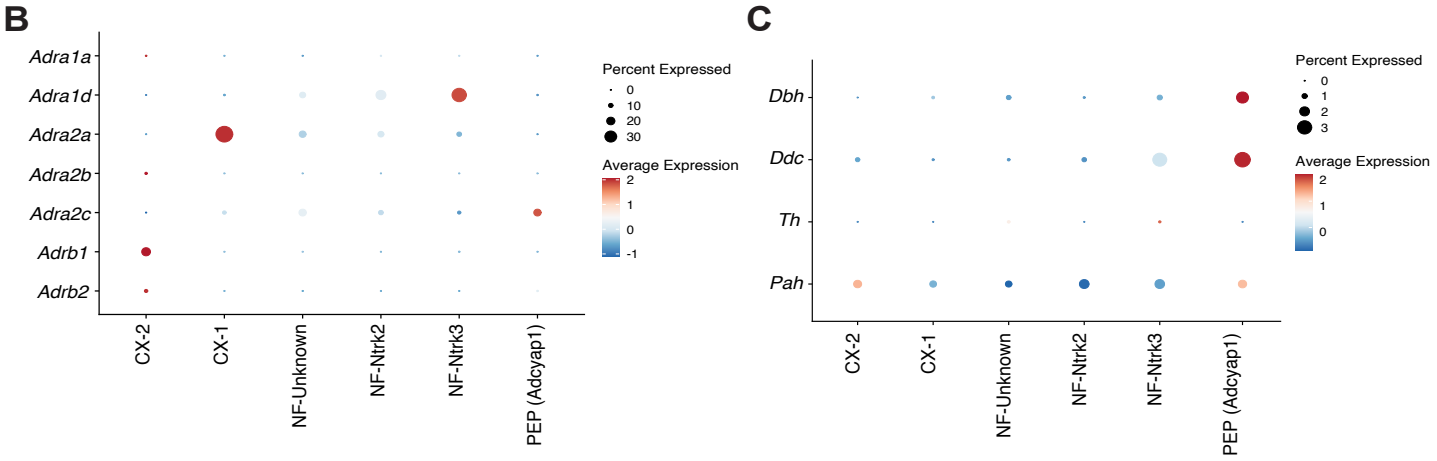

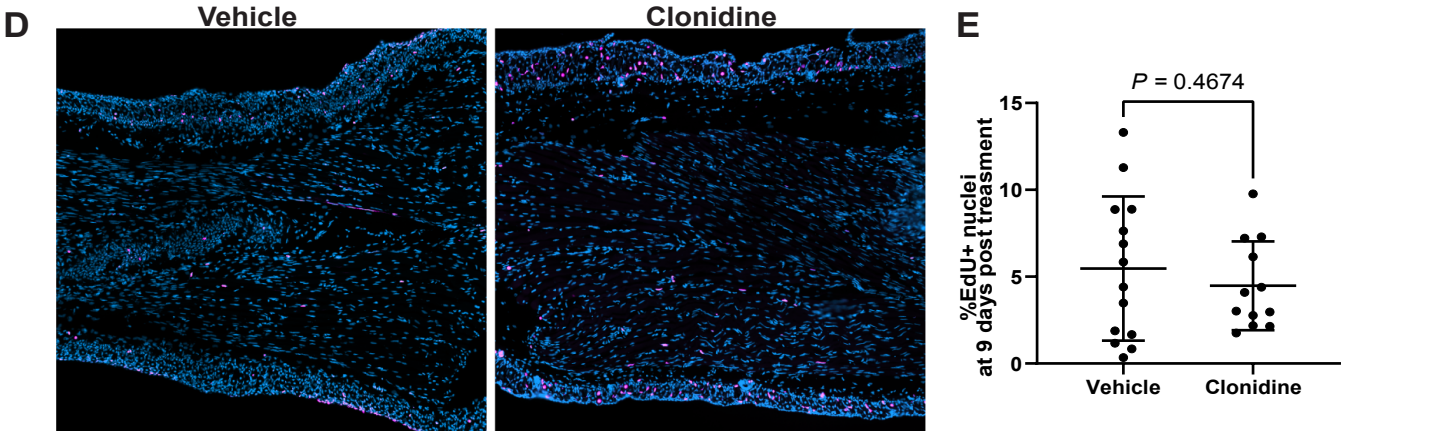

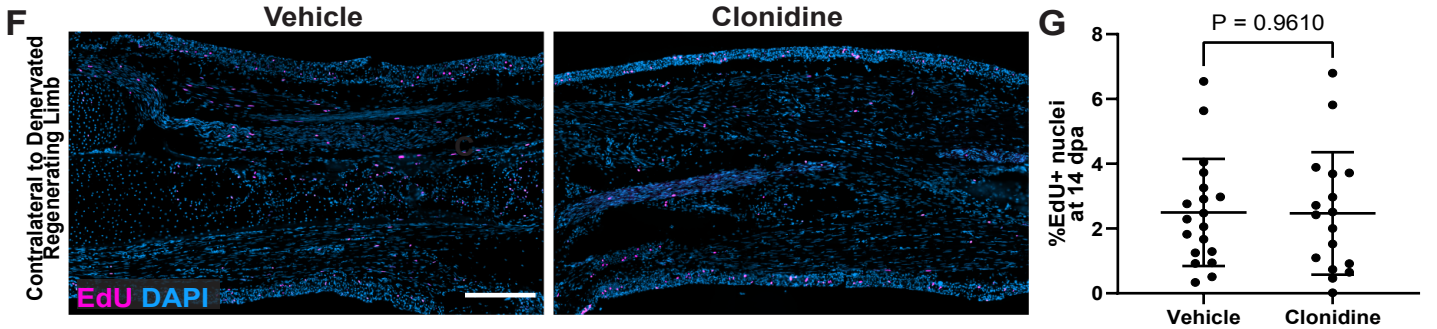

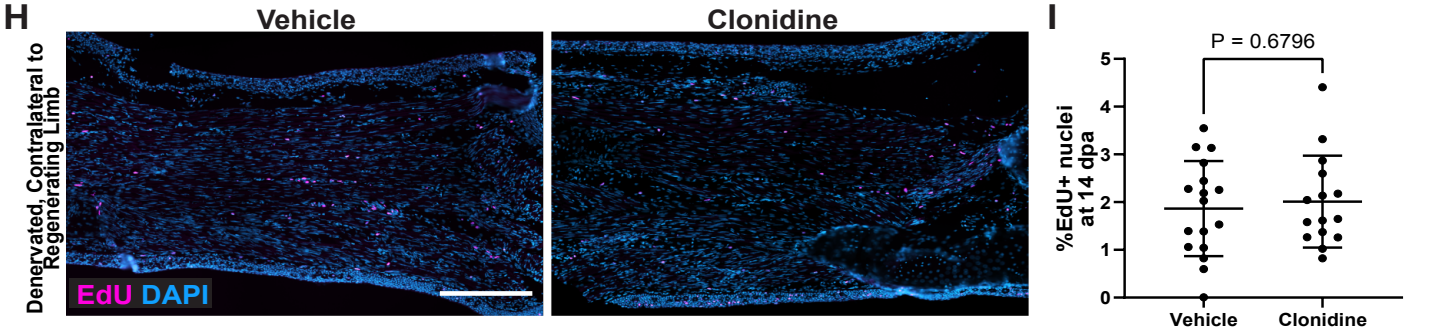

Supplementary Figure S1, related to Figure 3

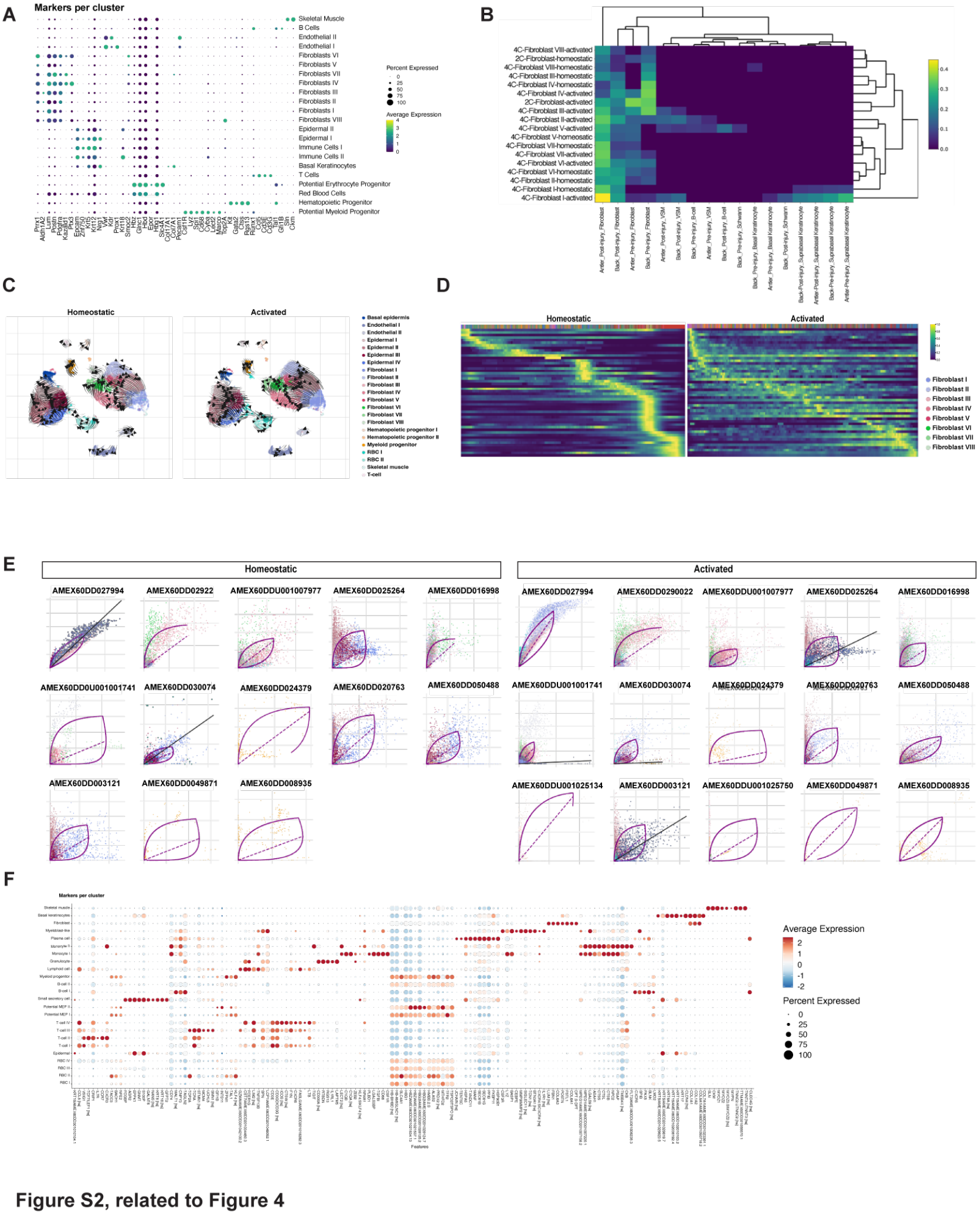

Figure S2, related to Figure 4

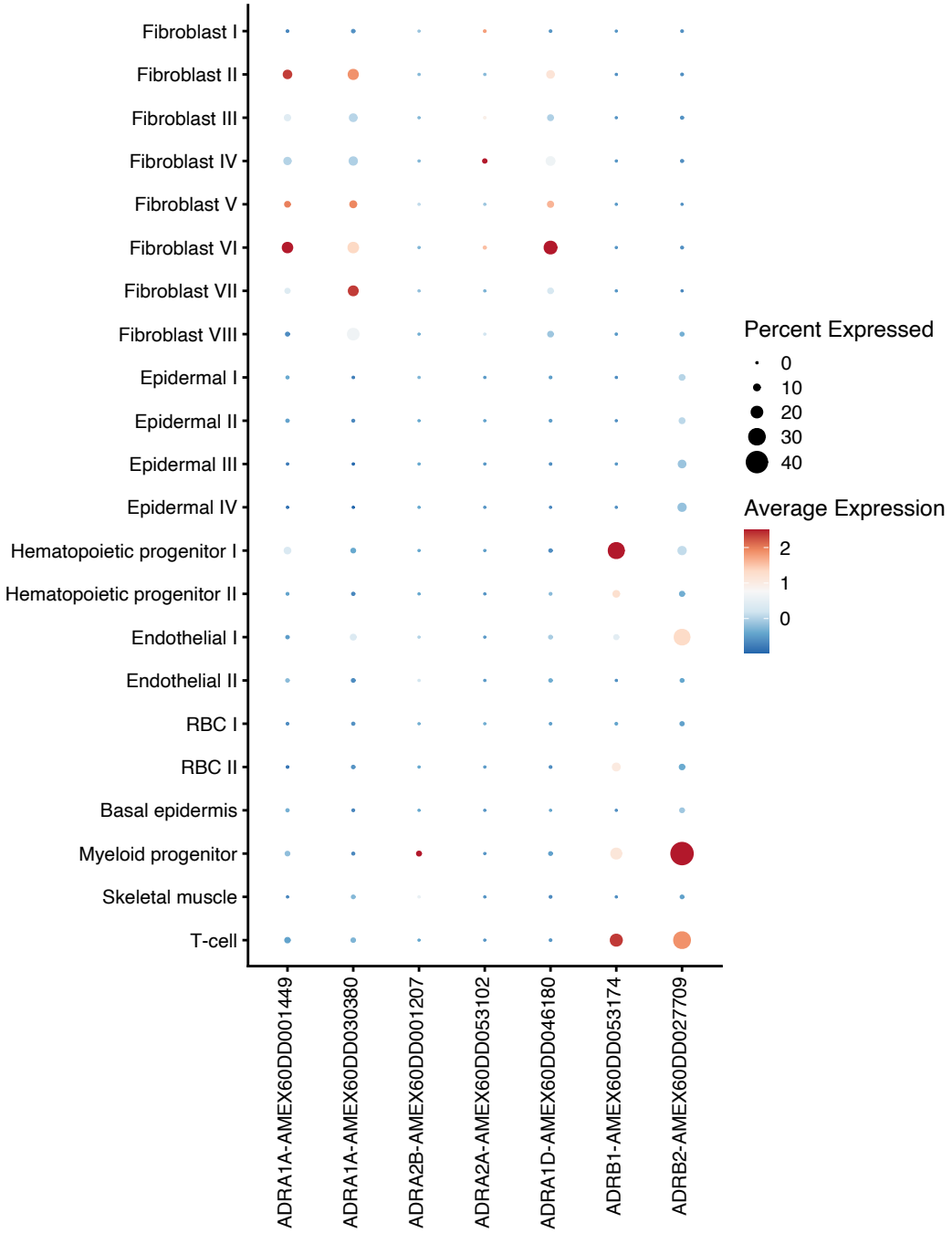

Figure S3, related to Figure 4

Figure S4, related to Figure 5

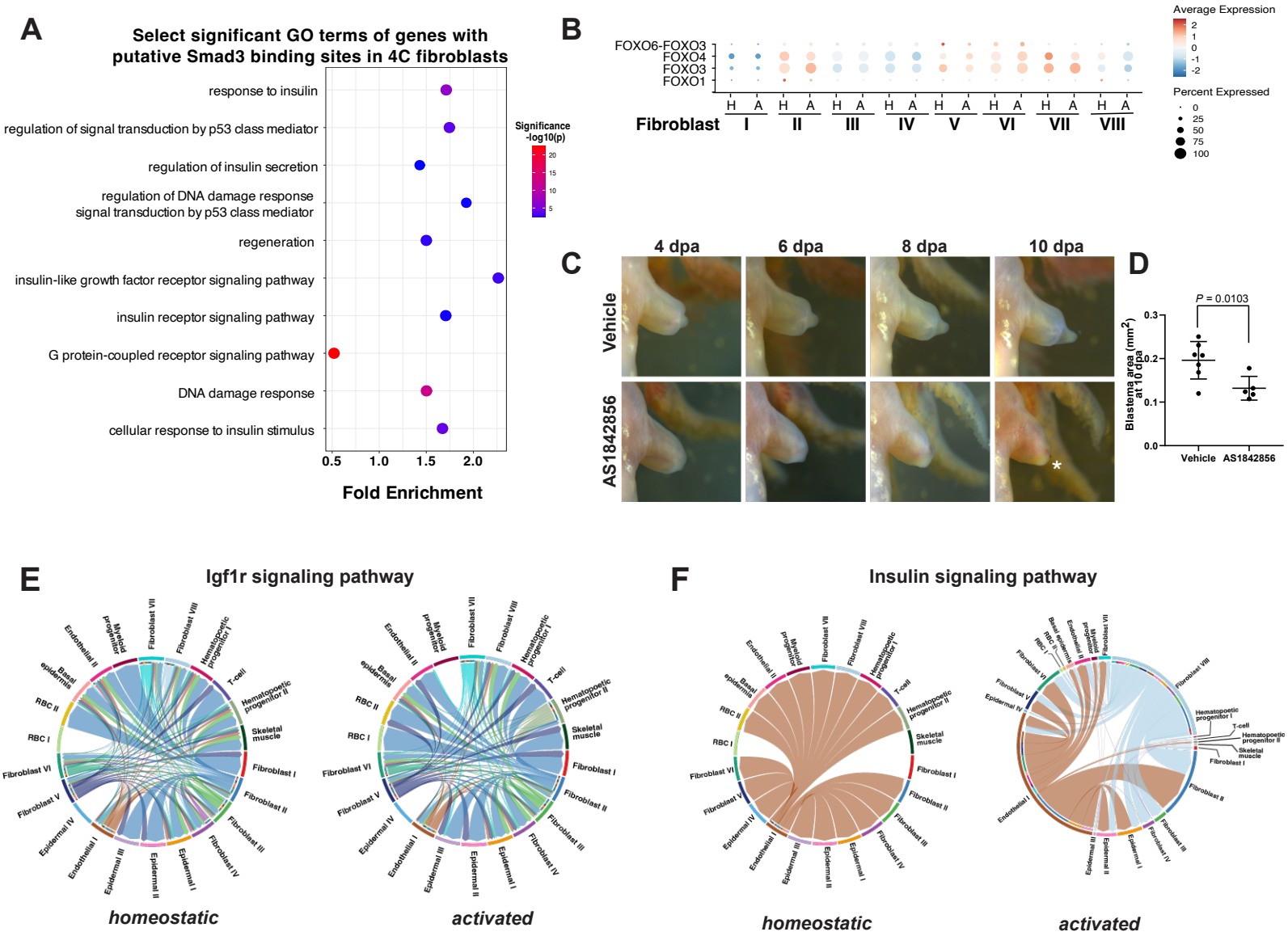

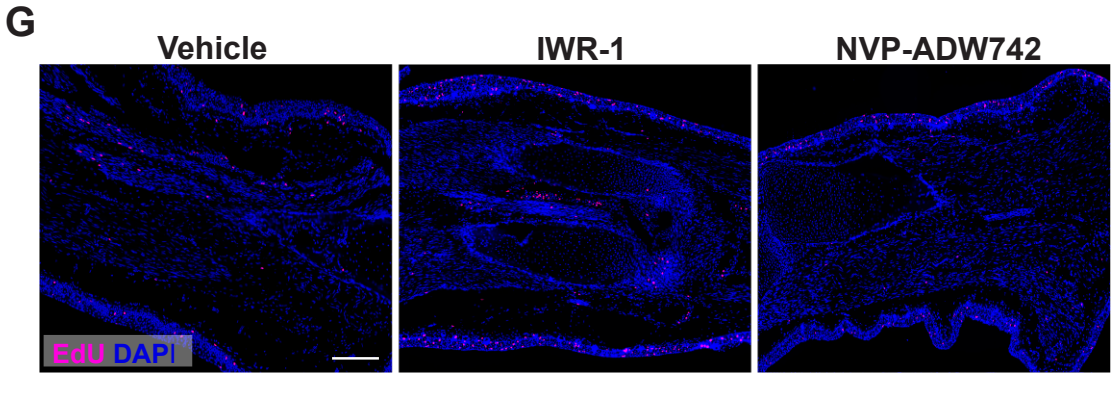

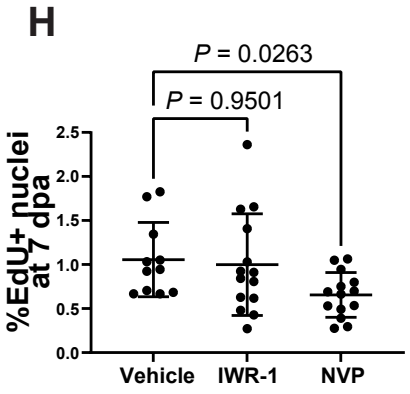

Figure S5, related to Figure 5

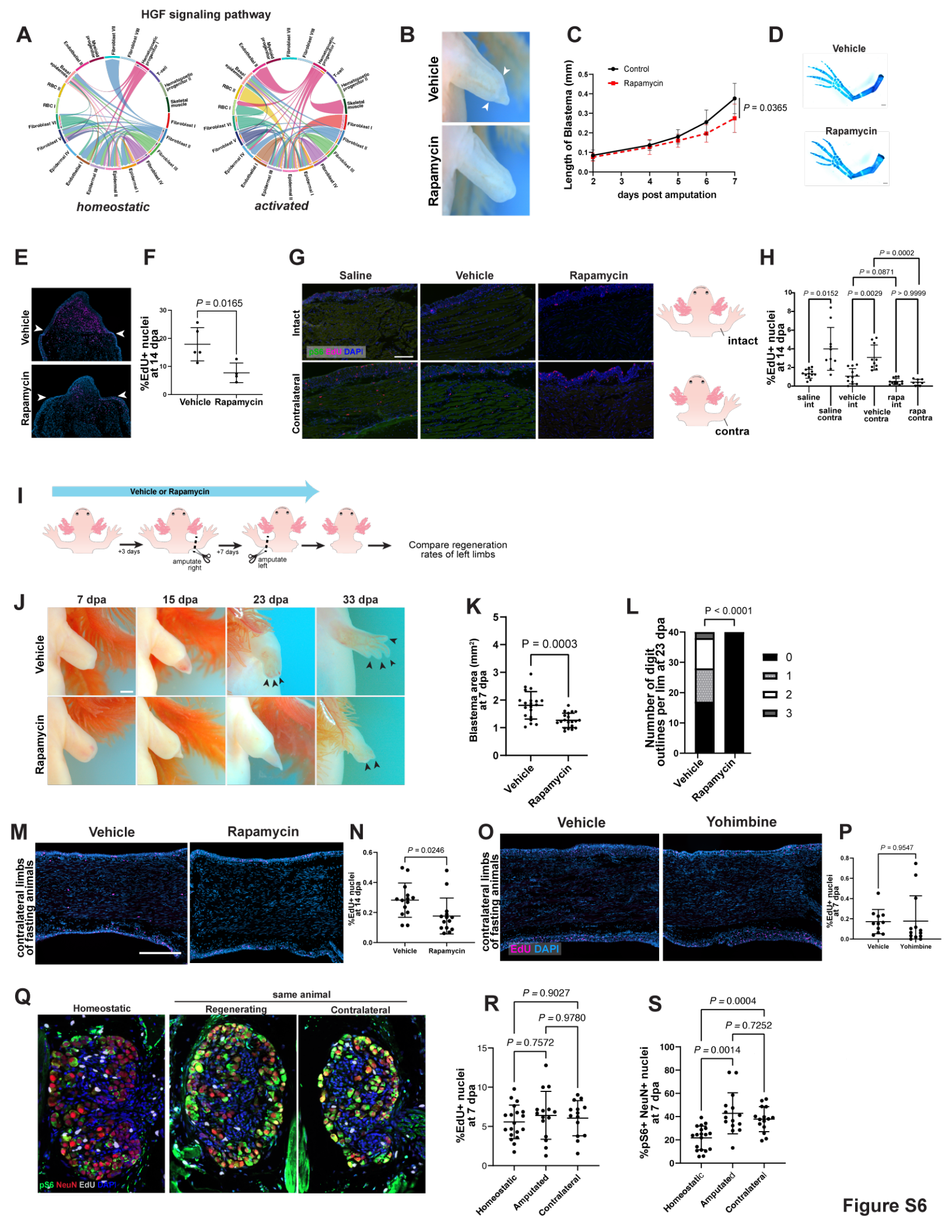
HGF signaling pathway
A
homeostatic
activated
B
Vehicle
Rapamycin
C
Control
Rapamycin
Length of Blastema (mm)
days post amputation
P = 0.0365
D
Vehicle
Rapamycin
E
Vehicle
Rapamycin
F
P = 0.0165
%EdU+ nuclei at 14 dpa
Vehicle
Rapamycin
G
Saline
Vehicle
Rapamycin
Intact
Contralateral
pS6 EdU DAPI
intact
contra
H
P = 0.0002
P = 0.0871
P = 0.0152
P = 0.0029
P > 0.9999
%EdU+ nuclei at 14 dpa
saline int
saline contra
vehicle int
vehicle contra
rapa int
rapa contra
I
Vehicle or Rapamycin
+3 days
amputate right
+7 days
amputate left
Compare regeneration rates of left limbs
J
7 dpa
15 dpa
23 dpa
33 dpa
Vehicle
Rapamycin
K
P = 0.0003
Blastema area (mm²) at 7 dpa
Vehicle
Rapamycin
L
P < 0.0001
Numnber of digit outlines per lim at 23 dpa
0
1
2
3
Vehicle
Rapamycin
M
Vehicle
Rapamycin
contralateral limbs of fasting animals
N
P = 0.0246
%EdU+ nuclei at 14 dpa
Vehicle
Rapamycin
O
Vehicle
Yohimbine
contralateral limbs of fasting animals
EdU DAPI
P
P = 0.9547
%EdU+ nuclei at 7 dpa
Vehicle
Yohimbine
Q
same animal
Homeostatic
Regenerating
Contralateral
pS6 NeuN EdU DAPI
R
P = 0.9027
P = 0.9780
P = 0.7572
%EdU+ nuclei at 7 dpa
Homeostatic
Amputated
Contralateral
S
P = 0.0004
P = 0.7252
P = 0.0014
%pS6+ NeuN+ nuclei at 7 dpa
Homeostatic
Amputated
Contralateral

Figure S6